Analysis of aerosol interactions with numerical techniques for solving coagulation, nucleation, condensation, dissolution, and reversible chemistry among multiple size distributions

Mark Z. Jacobson

Department of Civil and Environmental Engineering, Stanford University, Stanford, California, USA

Received 28 December 2001; revised 11 March 2002; accepted 13 March 2002; published 2 October 2002.

[1] This paper describes new and modified numerical techniques for solving the size- and time-dependent aerosol processes of nucleation, coagulation, condensation, dissolution, and reversible chemistry among multiple aerosol particle size distributions and the gas phase and over the entire relative humidity (RH) range. The techniques treat particle number, mole, and volume concentrations, solution and nonsolution densities, and refractive index consistently. Some findings include the following: (1) Coagulation internally mixes particles of different original composition over the entire size distribution. (2) Coagulation internally mixes a greater fraction of larger than smaller particles. (3) Coagulation internally mixes larger particles with more other distributions than it does smaller particles. (4) Coagulation among multiple distributions produces the same summed size distribution as coagulation of a single distribution when the sum of initial distributions is the same in both cases. (5) In a competition for vapor between homogeneous nucleation and condensation, the relative importance of condensation increases with an increasing number of background particles. (6) In the absence of a continuous source of new particles, coagulation, condensation, dissolution, hydration, and chemical reaction internally mix most particles within half a day under moderately polluted conditions. (7) Condensation increases the fractional coating of small more than large particles. (8) The real refractive index of a particle containing electrolytes is higher at low RHs than at high RHs. (9) The difference between total particle and solution real refractive indices increases with decreasing RH. (10) A solution real refractive index generally increases with decreasing particle size. *INDEX TERMS:* 0305 Atmospheric Composition and Structure: Aerosols and particles (0345, 4801); 0345 Atmospheric Composition and Structure: Pollution—urban and regional (0305); 0360 Atmospheric Composition and Structure: Transmission and scattering of radiation; 0365 Atmospheric Composition and Structure: Troposphere—composition and chemistry; 1610 Global Change: Atmopshere (0315, 0325); *KEYWORDS:* aerosols, coagulation, condensation, nucleation, equilibrium, internal mixtures

Citation: Jacobson, M. Z., Analysis of aerosol interactions with numerical techniques for solving coagulation, nucleation, condensation, dissolution, and reversible chemistry among multiple size distributions, *J. Geophys. Res.*, *107*(D19), 4366, doi:10.1029/2001JD002044, 2002.

1. Introduction

[2] Many studies to date have described numerical techniques for solving the differential coagulation equation [e.g., *Lushnikov*, 1975; *Turco et al.*, 1979; *Suck and Brock*, 1979; *Gelbard and Seinfeld*, 1980; *Tsang and Brock*, 1982; *Seigneur*, 1982; *Friedlander*, 1983; *Warren and Seinfeld*, 1985; *Tzivion et al.*, 1987; *Toon et al.*, 1988; *Strom et al.*, 1992; *Kim and Seinfeld*, 1992; *Jacobson et al.*, 1994; *Kostoglou and Karabelas*, 1994; *Jacobson and Turco*, 1995; *Binkowski and Shankar*, 1995; *Kumar and Ramkrishna*, 1996; *Fassi-Fihri et al.*, 1997; *Russell and Seinfeld*, 1998; *Trautmann and Wanner*, 1999; *Fernandez-Diaz et al.*, 2000; *Bott*, 2000; *Jeong and Choi*, 2001; *Sandu*, 2002]. Many studies have also examined solutions to condensational growth equations [e.g., *Mordy*, 1959; *Middleton and Brock*, 1976; *Gelbard and Seinfeld*, 1980; *Varoglu and Finn*, 1980; *Smolarkiewicz*, 1983; *Friedlander*, 1983; *Tsang and Brock*, 1986; *Whitby*, 1985; *Brock et al.*, 1986; *Tsang and Korgaonkar*, 1987; *Toon et al.*, 1988; *Rao and McMurry*, 1989; *Tsang and Huang*, 1990; *Gelbard*, 1990; *Pilinis*, 1990; *Kim and Seinfeld*, 1990, 1992; *Jacobson and Turco*, 1995; *Lister et al.*, 1995; *Binkowski and Shankar*, 1995; *Jacobson*, 1997c; *Kleeman et al.*, 1997; *Gelbard et al.*, 1998; *Chock and Winkler*, 2000; *Nguyen and Dabdub*, 2001; *Sandu and Borden*, 2001]. A third group of studies has examined solutions to equations for nonequilibrium dissolutional growth plus equilibrium reversible chemistry of electrolytes [*Jacobson et al.*, 1996; *Meng and Seinfeld*,

0148-0227/02/2001JD002044$09.00

1996; *Jacobson*, 1997a, 1997b, 1997c; *Meng et al.*, 1998; *Sun and Wexler*, 1998a, 1998b; *Song and Carmichael*, 1999; *von Salzen and Schlünzen*, 1999; *Capaldo et al.*, 2000; *Pilinis et al.*, 2000].

[3] In most studies to date, one aerosol size distribution has been considered. In some studies, more than one distribution has been considered [e.g., *Toon et al.*, 1988; *Jacobson et al.*, 1994; *Fassi-Fihri et al.*, 1997; *Kleeman et al.*, 1997; *Russell and Seinfeld*, 1998; *Jacobson*, 2001]. One reason to treat multiple distributions and interactions among them is that real particles exist in a variety of mixing states [e.g., *Andreae et al.*, 1986; *Levin et al.*, 1996; *Murphy et al.*, 1998; *Pósfai et al.*, 1999; *Silva et al.*, 2000; *Guazzotti et al.*, 2001; *Okada and Hitzenberger*, 2001; *Naoe and Okada*, 2001]. Particles near their sources are generally externally mixed, whereas those far from their sources are often partially or completely internally mixed. When only one size distribution is treated in a model, all material is considered internally mixed at the emission source. Such a representation can distort predicted chemical compositions [e.g., *Kleeman et al.*, 1997]. When multiple distributions without interactions among them are treated, all distributions are treated as externally mixed. This is unrealistic away from source regions. When multiple distributions with interactions among them are treated, some distributions can be treated as externally mixed whereas others can be treated as partially or completely internally mixed. The radiative effects of externally and internally mixed particles differ. For example, the modeled global direct radiative forcing of black carbon (BC) may be about a factor of two higher when BC is treated as an internally mixed core surrounded by a shell compared with when it is treated as externally mixed [*Jacobson*, 2000]. Simulations of the global scale mixing state and resulting direct forcing of BC (which used the numerical techniques and size distributions treated here) suggest that both may fall between those of an external and internal mixture but closer to those of an internal mixture [*Jacobson*, 2001].

[4] In this paper, techniques for solving (1) coagulation, (2) nucleation/condensational growth simultaneously, and (3) coupled nonequilibrium dissolutional growth/equilibrium reversible chemistry of electrolytes, all between the gas phase and multiple aerosol size distributions, are given. All techniques conserve moles or volume (including between the gas and aerosol phases), all techniques except the reversible chemistry technique are noniterative, and all techniques are unconditionally stable (where a stable solution is defined as one in which the difference between the numerical and exact solution is bounded regardless of the time step or integration time [e.g., *Celia and Gray*, 1992, p. 216]). The techniques make use of a consistent treatment of particle number concentration, mole concentration, volume concentration, solution density, nonsolution density, and refractive index.

[5] In the following sections, the numerical techniques are described. The techniques are then analyzed in box model simulations to explore physical processes, chemical processes, and interactions affecting aerosol particle evolution. In one case, results are compared when a different method of treating the aerosol size distribution is considered. Equations for the calculation of particle real and imaginary refractive from compositions in multiple distributions are also given.

2. Particle Size Distributions

[6] The numerical treatments here assume that particles can be described by any number of size distributions, each with any number of size bins and any number of components within each size bin. Each size bin i in each size distribution N is characterized by a number concentration, n_{Ni} (number of particles per cubic centimeter of air). Each component q in each size bin of each distribution is characterized by a mole concentration, $c_{q,Ni}$ (moles per cubic centimeter of air).

[7] For many processes, such as coagulation, single-particle volume information is needed. The calculation of single-particle volume takes into account the facts that particles contain a solution and nonsolution component and solution density varies as a function of electrolyte concentration. Single-particle volumes (cubic centimeters per particle) are calculated as

$$\upsilon_{Ni} = \frac{v_{Ni}}{n_{Ni}} \tag{1}$$

where v_{Ni} is the volume concentration (cubic centimeters of particle per cubic centimeter of air) of the total particle and is calculated as

$$v_{Ni} = v_{s,Ni} + \sum_{q=1}^{N_{NS}} v_{q,Ni} = v_{s,Ni} + \sum_{q=1}^{N_{NS}} \frac{m_q}{\rho_q} c_{q,Ni} \tag{2}$$

where $v_{s,Ni}$ is the volume concentration of the solution, N_{NS} is the number of nonsolution components, $v_{q,Ni} = m_q c_{q,Ni}/\rho_q$ is the volume concentration of each nonsolution component, m_q is the molecular weight (grams per mole) of component q, and ρ_q is the mass density (grams per cubic centimeter) of component q.

[8] The volume concentration of a solution is calculated as

$$v_{s,Ni} = \frac{\boldsymbol{m}_{s,Ni}}{\rho_{s,Ni}} \tag{3}$$

where

$$\boldsymbol{m}_{s,Ni} = m_v c_{w,Ni} + \sum_{q=1}^{N_S} m_q c_{q,Ni} \tag{4}$$

is the mass concentration (grams per cubic centimeter of air) of the solution (m_v is the molecular weight of water and $c_{w,Ni}$ is the mole concentration of liquid water) and

$$\rho_{s,Ni} = \frac{1}{\sum_{q=1}^{N_E} \frac{\chi_{q,Ni}}{\rho_{a,q,Ni}}} \tag{5}$$

is the mass density (grams per cubic centimeter of solution) of the solution [e.g., *Tang*, 1997]. In equations (4) and (5),

Table 1a. Components in and Sources of New Particles in Each Size Distribution

Distribution Name	Symbol	Potential Components	Initialized?	Sources of New Particles
Sea spray	A	All in (b) except BC, OM, and soil	Yes	Em[a]
Soil	B	All except BC, OM, and species with Na, Ca, Mg, K	Yes	Em
Sulfate	D	All except BC, OM, soil, and species with Na, Ca, Mg, K	Yes	Nuc
BC with 0–5% shell	E1	All except OM, soil, and species with Na, Ca, Mg, K	Yes	Em
BC with 5–20% shell	E2	All except OM, soil, and species with Na, Ca, Mg, K	–	Gr from E1
BC with >20% shell	E3	All except OM, soil, and species with Na, Ca, Mg, K	–	Gr from E1 and E2
OM	F	All except BC, soil, and species with Na, Ca, Mg, K	Yes	Em
Sea spray–soil	AB	All except BC and OM	–	Co
Sea spray–sulfate	AD	All except BC, OM, soil	–	Co
Sea spray–BC	AE	All except OM and soil	–	Co
Sea spray–OM	AF	All except BC and soil	–	Co
Soil–sulfate	BD	All except BC, OM, and species with Na, Ca, Mg, K	–	Co
Soil–BC	BE	All except OM, and species with Na, Ca, Mg, K	–	Co
Soil–OM	BF	All except BC and species with Na, Ca, Mg, K	–	Co
Sulfate–BC	DE	All except OM, soil, and species with Na, Ca, Mg, K	–	Co
Sulfate–OM	DF	All except BC, soil, and species with Na, Ca, Mg, K	–	Co
BC–OM	EF	All except soil, and species with Na, Ca, Mg, K	–	Co
Internal mixture	MX	All	–	Co

[a] Em = emissions, Nuc = homogeneous nucleation, Co = coagulation, Gr = condensational and/or dissolutional growth. All distributions are affected by self-coagulation loss to larger sizes and heterocoagulation loss to other distributions (except the MX distribution, which has no heterocoagulation loss). In addition, particles in all distributions can grow in size by condensation and dissolution, reversible equilibrium chemistry, and equilibrium hydration. The difference between distributions A and AD is that the only source of new A particles is emissions, whereas that of new AD particles is coagulation of A with D, A with AD, or D with AD particles. The differences among distributions E1, E2, E3, and DE are that the only source of new E1 particles is emissions, the only sources of E2 and E3 particles are growth from E1 and E2, respectively, and the only source of new DE particles is coagulation of E1, E2, or E3 with D or DE and coagulation of D with DE. Each size distribution contains multiple size bins.

N_S is the number of electrolytes in the solution. In equation (5),

$$\chi_{q,Ni} = \frac{m_q c_{q,Ni}}{\boldsymbol{m}_{s,Ni}} \tag{6}$$

is the mass fraction of component q in solution and $\rho_{a,\,q,\,Ni}$ is the mass density of electrolyte q as if it were alone in solution at the same weight percent as the current weight percent of total solute. Density polynomials for several electrolytes are available in the work of *Tang* [1997].

[9] The numerical methods described here assume that each distribution can be affected by nucleation, emissions, coagulation, condensation, dissolution, chemical equilibrium, transport, and removal (although emissions, transport, and removal are not simulated here). Table 1a shows a set of 18 size distributions used here for all the simulations discussed. Table 1b lists the components treated in each distribution of Table 1a, except as specified in Table 1a. For each distribution, 60 size bins, ranging from 0.001 to 120 μm in radius, are used. In sum, this study considers 32,400 concentrations in a single spatial grid cell (18 size distributions × an average of 30 species per distribution × 60 size bins per species per distribution).

[10] Table 1a identifies the sources of new particles in each distribution. For four distributions (A, B, E1, and F), the only source of new particles is emissions. For one distribution (D), the only source of new particles is homogenous nucleation. For 12 distributions (AB, AD, AE, AF, BD, BE, BF, DE, DF, EF, and MX), the only new-particle source is coagulation between simpler distributions. For two distributions (E2 and E3), the only new-particle source is condensation onto E1 or E2, respectively. Distributions E1, E2, and E3 contain black carbon (BC) with different volume fractional coatings (0–5%, 5–20%, and >20%, respectively). BC is emitted into (and initialized in) distribution E1. When the fractional coating of E1 particles in a size bin increases above 5% during growth, all particles in the bin are moved to distribution E2, and so on. This allows distribution E1 to always contain relatively externally mixed BC. All distributions (including E1, E2, and E3) are affected by self-coagulation loss to larger sizes and heterocoagulation loss to other distributions (except for the MX distribution, which has no heterocoagulation loss). Particles in all distributions can grow by condensation, dissolution, and equilibrium hydration, and can be affected by chemistry.

[11] Each size bin in each size distribution is characterized by a high- and low-edge volume, which equal a constant, V_{rat}, multiplied by the high- and low-edge volume, respectively, of the next-smallest bin. One way to initialize the high- and low-edge volume of a bin is given by *Jacobson* [1999a, equations (14.6) and (14.7)]. Other ways are also possible. All particles in the bin, though, have a single characteristic volume (υ_{Ni}) between the low- and high-edge volumes of the bin. This single volume can change as the particles grow, evaporate, coagulate, etc. If

Table 1b. Aerosol Components in Each Distribution of Table 1a, Except as Specified in That Table

Species Formula	Species Formula	Species Formula
H_2O(aq)	CO_3^{2-}	$KHSO_4$(s)
H_2CO_3(aq)	NH_4NO_3(s)	K_2SO_4(s)
H_2SO_4(aq)	NH_4Cl(s)	K_2CO_3(s)
H^+	NH_4HSO_4(s)	$Ca(NO_3)_2$(s)
NH_4^+	$(NH_4)_2SO_4$(s)	$CaCl_2$(s)
Na^+	$(NH_4)_3H(SO_4)_2$(s)	$CaSO_4$(s)
Mg^{2+}	$(NH_4)_2CO_3$(s)	$CaCO_3$(s)
Ca^{2+}	$NaNO_3$(s)	$Mg(NO_3)_2$(s)
K^+	NaCl(s)	$MgCl_2$(s)
HSO_4^-	$NaHSO_4$(s)	$MgSO_4$(s)
SO_4^{2-}	Na_2SO_4(s)	$MgCO_3$(s)
NO_3^-	Na_2CO_3(s)	Soil
Cl^-	KNO_3(s)	BC
HCO_3^-	KCl(s)	OM

the volume increases above the high-edge volume of the bin, all particles in the bin are moved to and averaged with particles in the next-largest bin. This size bin structure is the moving-center structure [*Jacobson*, 1997a, 1999a, pp. 420–4201]. Results from it have been compared with other size structures by *Jacobson* [1997a] and *Zhang et al.* [1999] and are compared further here with those from another structure, the full-moving structure.

3. Coagulation

[12] The coagulation scheme described here is an extension of an earlier volume-conserving, noniterative, unconditionally stable coagulation scheme in which multiple size distributions were considered [*Jacobson et al.*, 1994]. When external mixtures coagulated in the original scheme, they were sent into a single internally mixed distribution. For this work, the scheme was modified to treat coagulation into and among any number of externally mixed, binary, ternary, etc. combinations of distributions and any number of components in each distribution (maintaining volume conservation). In the work of *Jacobson et al.* [1994], results from the scheme were compared with analytical and numerical solutions for one distribution. There are no analytical solutions available for multiple distributions, but it can be shown mathematically and from numerical simulations that coagulation within and among multiple distributions gives the same solution, summed over all distributions, as coagulation within one distribution if the initial volume concentrations, summed over all distributions, are the same in both cases. As such, the accuracy of the multiple-distribution solution is exactly the same as the single-distribution solution. Coagulation rate coefficients treated here include those for Brownian motion, Brownian diffusion enhancement, gravitational collection, turbulent inertial motion, and turbulent shear [e.g., *Jacobson*, 1999a, Figure 16.4 and equations (16.28)–(16.34)].

[13] The volume-conserving solution to coagulation among any number of size distributions, size bins in each distribution, and component in each distribution is given as follows. The final number concentration of particles in bin k of distribution N at time t is

$$n_{Nk,t} = \frac{n_{Nk,t-h} + h(T_1 + T_2)}{1 + hT_3}$$

$$T_1 = \frac{1}{\upsilon_{Nk,t-h}} \sum_{M=1}^{N_T} \left[P_{N,M} \sum_{j=1}^{k} \cdot \left(n_{Mj,t-h} \sum_{i=1}^{k-1} f_{Ni,Mj,Nk,t-h} \beta_{Ni,Mj,t-h} \upsilon_{Ni,t-h} n_{Ni,t} \right) \right]$$

$$T_2 = \frac{1}{\upsilon_{Nk,t-h}} \sum_{M=1}^{N_T} \sum_{I=1}^{N_T} \left[Q_{I,M,N} \sum_{j=1}^{k} \cdot \left(n_{Mj,t-h} \sum_{i=1}^{k} f_{Ii,Mj,Nk,t-h} \beta_{Ii,Mj,t-h} \upsilon_{Ii,t-h} n_{Ii,t} \right) \right] \quad (7)$$

$$T_3 = \sum_{j=1}^{N_B} \left[\sum_{M=1}^{N_T} \left[(1 - L_{N,M}) \cdot (1 - f_{Nk,Mj,Nk,t-h}) + L_{N,M} \right] \beta_{Nk,Mj,t-h} n_{Mj,t-h} \right]$$

where h is the time step size, $t - h$ indicates a value at the beginning of the time step, N_T is the total number of size distributions (18 in Tables 1a and 1b), N_B is the number of size bins in each distribution, $\beta_{Ni,Mj,t-h}$ is the coagulation rate coefficient (cubic centimeters per particle per second) between a particle in size bin i of distribution N and a particle in bin j of distribution M, and $f_{Ii,Mj,Nk,t-h}$ is the fraction of the summed single-particle volume $V_{Ii,Mj,t-h} = \upsilon_{Ii,t-h} + \upsilon_{Mj,t-h}$ partitioned into bin k of distribution N at the beginning of the time step. This formulation allows the average single-particle volume (υ) of a particle in a size bin to change each time step, which is necessary for the moving-center size structure, in which the single-particle volume in a bin can vary between the low- and high-edge volume in the bin. For a size bin structure in which single-particle volume does not change in time (e.g., a stationary structure), the volume fractions are calculated only once, at the beginning of the simulation. In either case, volume fractions are calculated as

$$f_{Ii,Mj,Nk,t-h} = \begin{cases} \left(\frac{\upsilon_{Nk+1,t-h} - V_{Ii,Mj,t-h}}{\upsilon_{Nk+1,t-h} - \upsilon_{Nk,t-h}} \right) \frac{\upsilon_{Nk,t-h}}{V_{Ii,Mj,t-h}} & \upsilon_{Nk,t-h} \le V_{Ii,Mj,t-h} < \upsilon_{Nk+1,t-h} \quad k < N_B \\ 1 - f_{Ii,Mj,Nk-1,t-h} & \upsilon_{Nk,t-h} < V_{Ii,Mj,t-h} < \upsilon_{Nk,t-h} \quad k > 1 \\ 1 & V_{Ii,Mj,t-h} \ge \upsilon_{Nk,t-h} \quad k = N_B \\ 0 & \text{all other cases} \end{cases} \quad (8)$$

[14] Finally, P, Q, and L in equation (7) are either 1 or 0, depending on the coagulation interactions accounted for. The values are illustrated by considering Table 2, which identifies a possible set of coagulation interactions among the distributions in Tables 1a and 1b. The parameter $P_{N,M} = 1$ if particles in distribution N coagulating with particles in distribution M produce larger particles in distribution N. For example, sea spray–soil (AB) plus sea spray (A) produces more sea spray–soil (AB); thus, $P_{AB,A} = 1$. The parameter $Q_{I,M,N} = 1$ if particles in distribution I coagulating with particles in distribution M produce particles in distribution N, where $I \neq M$ and $I \neq N$. For example, soil (B) plus sulfate (D) produces soil–sulfate (BD); thus, $Q_{B,D,BD} = 1$. The parameter $L_{N,M} = 1$ if particles in distribution N coagulating with particles in distribution M do not produce particles in distribution N. For example, soil (B) plus sulfate (D) does not produce soil (B); thus, $L_{B,D} = 1$. On the other hand, soil–sulfate (BD) plus sulfate (D) produces soil–sulfate (BD); thus, $L_{BD,D} = 0$ in that case.

[15] In equation (7), term T_1 accounts for production into distribution N due to self-coagulation (e.g., $N + N$) and heterocoagulation of N with a simpler distribution M. Term T_2 accounts for production into distribution N due to heterocoagulation of two independent distributions, I and M. The first part of term T_3 accounts for both self-coagulation loss ($N + N$) and heterocoagulation loss ($N + M$) to larger sizes of the same distribution (N). The second part of T_3 accounts for heterocoagulation loss ($N + M$) to any distribution aside from N.

[16] Volume concentrations of each individual component q in size bin k of distribution N are similarly solved with

$$v_{q,Nk,t} = \frac{v_{q,Nk,t-h} + h(T_1 + T_2)}{1 + hT_3}$$

Table 2. Coagulation Interactions

Size Distribution Name	Symbol	Symbol of Second Distribution																	
		A	B	D	E1	E2	E3	F	AB	AD	AE	AF	BD	BE	BF	DE	DF	EF	MX
Sea spray	A	A	AB	AD	AE	AE	AE	AF	AB	AD	AE	AF	MX	MX	MX	MX	MX	MX	MX
Soil	B	AB	B	BD	BE	BE	BE	BF	AB	MX	MX	MX	BD	BE	BF	MX	MX	MX	MX
Sulfate	D	AD	BD	D	DE	DE	DE	DF	MX	AD	MX	MX	BD	MX	MX	DE	DF	MX	MX
BC with 0–5% shell	E1	AE	BE	DE	E1	E2	E3	EF	MX	MX	AE	MX	MX	BE	MX	DE	MX	EF	MX
BC with 5–20% shell	E2	AE	BE	DE	E2	E2	E3	EF	MX	MX	AE	MX	MX	BE	MX	DE	MX	EF	MX
BC with >20% shell	E3	AE	BE	DE	E3	E3	E3	EF	MX	MX	AE	MX	MX	BE	MX	DE	MX	EF	MX
OM	F	AF	BF	DF	EF	EF	EF	F	MX	MX	MX	AF	MX	MX	BF	MX	DF	EF	MX
Sea spray–soil	AB	AB	AB	MX	MX	MX	MX	MX	AB	MX	MX	MX	MX	MX	MX	MX	MX	MX	MX
Sea spray–soil	AD	AD	MX	AD	MX	MX	MX	MX	MX	AD	MX	MX	MX	MX	MX	MX	MX	MX	MX
Sea spray–BC	AE	AE	MX	MX	AE	AE	AE	MX	MX	MX	AE	MX	MX	MX	MX	MX	MX	MX	MX
Sea spray–OM	AF	AF	MX	MX	MX	MX	MX	AF	MX	MX	MX	AF	MX	MX	MX	MX	MX	MX	MX
Soil–AS	BD	MX	BD	BD	MX	MX	MX	MX	MX	MX	MX	MX	BD	MX	MX	MX	MX	MX	MX
Soil–BC	BE	MX	BE	MX	BE	BE	BE	MX	MX	MX	MX	MX	MX	BE	MX	MX	MX	MX	MX
Soil–OM	BF	MX	BF	MX	MX	MX	MX	BF	MX	MX	MX	MX	MX	MX	BF	MX	MX	MX	MX
Sulfate–BC	DE	MX	MX	DE	DE	DE	DE	MX	MX	MX	MX	MX	MX	MX	MX	DE	MX	MX	MX
Sulfate–OM	DF	MX	MX	DF	MX	MX	MX	DF	MX	MX	MX	MX	MX	MX	MX	MX	DF	MX	MX
BC–OM	EF	MX	MX	MX	EF	EF	EF	EF	MX	MX	MX	MX	MX	MX	MX	MX	MX	EF	MX
Internal mixture	MX	MX	MX	MX	MX	MX	MX	MX	MX	MX	MX	MX	MX	MX	MX	MX	MX	MX	MX

The table gives the symbol of the size distribution into which two particles from either the same or different distributions coagulate to. For example, when a sea spray particle (A) coagulates with a soil particle (B), the resulting particle is a sea spray–soil (AB) particle. When three or more externally mixed (A. . .F) distributions or an externally mixed and binary (AB. . .EF) distribution or two binary distributions combine, they enter the mixed (MX distribution). Thus, the combination of OM (F) with sea spray–soil (AB) gives a mixed particle (MX).

$$T_1 = \sum_{M=1}^{N_T} \left[P_{N,M} \sum_{j=1}^{k} \cdot \left(n_{Mj,t-h} \sum_{i=1}^{k-1} f_{Ni,Mj,Nk,t-h} \beta_{Ni,Mj,t-h} v_{q,Ni,t} \right) \right]$$

$$T_2 = \sum_{M=1}^{N_T} \sum_{I=1}^{N_T} \left[Q_{I,M,N} \sum_{j=1}^{k} \cdot \left(n_{Mj,t-h} \sum_{i=1}^{k} f_{Ii,Mj,Nk,t-h} \beta_{Ii,Mj,t-h} v_{q,Ii,t} \right) \right] \quad (9)$$

$$T_3 = \sum_{j=1}^{N_B} \left[\sum_{M=1}^{N_T} \left[(1 - L_{N,M}) \cdot (1 - f_{Nk,Mj,Nk,t-h}) + L_{N,M} \right] \beta_{Nk,Mj,t-h} n_{Mj,t-h} \right]$$

[17] Equations (7) and (9) are solved independently of one another, but size distributions and bins must be solved in a special order for each equation. Distributions that have no coagulation production from other distributions are solved first, followed by distributions with production terms from previously solved distributions. For example, distributions A, B, D, E1, and F in Table 2 are solved first (in any order), followed by distribution E2, followed by distribution E3, followed by distributions AB, AD, AE, AF, BD, BE, BF, DE, DF, and EF (in any order), followed by distribution MX. Within each distribution, equations are solved from bin $k = 1 \ldots N_B$. The volume concentrations in equation (9) can be solved in any order. To minimize computer time, all calculations involving a zero value of f, P, or Q are eliminated ahead of time.

4. Nucleation, Condensation, Dissolution, and Reversible Chemistry

[18] Solutions to homogeneous nucleation, condensational growth, dissolutional growth, and reversible chemical reactions are discussed here. The difference between condensational and dissolutional growth is that condensational growth is calculated under the assumption that the saturation vapor mole concentration (SVMC) is fixed for a given set of meteorological or chemical conditions, whereas dissolutional growth is calculated under the assumption that the SVMC varies continuously according to the molality of the substance in solution. Previously, *Jacobson* [1997c, 1999a] developed two schemes, the Analytical Predictor for Condensation (APC) and Analytical Predictor for Dissolution (APD) schemes, which were noniterative, unconditionally stable methods for solving condensation and dissolution, respectively, between the gas phase and multiple size bins of an aerosol distribution. Predictions from these schemes were compared with integrated numerical solutions. The APC scheme was used to solve condensational growth of H_2O and relatively involatile species, such as H_2SO_4. The APD scheme was used to solve dissolutional growth of more volatile species, such as HCl, HNO_3, and NH_3. The APD scheme was coupled with a chemical equilibrium code, which was used to determine solubility terms for the growth equation.

[19] Here the APC and APD schemes were combined and modified to form a noniterative, unconditionally stable scheme for solving nucleation, condensation, and dissolution simultaneously between the gas phase and multiple size distributions. The schemes were also modified to treat solids in some size bins and the absence of solids in others. The revised technique is the APNCD (Analytical Predictor of Nucleation, Condensation, and Dissolution) scheme. The technique simplifies to the APD scheme for dissolution in size bins in which no solids form and to the APC scheme for condensation of involatile species [e.g., S(VI)] and for dissolution of volatile species in the presence of solids. The scheme simultaneously solves binary or homomolecular homogeneous nucleation, allowing growth and nucleation to compete for limited amounts of vapor.

[20] Although the APNCD scheme, itself, is noniterative, it relies on solubility and saturation vapor pressure terms calculated from an iterative equilibrium code. The chemical equilibrium code used is EQUISOLV II [*Jacobson*, 1999b]. The equilibrium code iterates temperature-dependent equilibrium, solute activity coefficient, and water activity coefficient equations among sodium, chloride, potassium, calcium, magnesium, sulfate, nitrate, chloride, and carbonate substances in the ionic, liquid, and/or solid phases from 0.1 to 99.5% relative humidity (RH).

[21] EQUISOLV II is used to calculate internal aerosol composition and LWC for use in saturation vapor pressure and solubility terms in the APNCD scheme. After the growth calculation, EQUISOLV II is used a second time to equilibrate gas-phase NH_3 with all ions and solids in all size bins of the aerosol phase to determine final aerosol composition for the time step. The reason for equilibrating, instead of growing, NH_3 is that growth of S(VI), HNO_3, and HCl results in the production of anions in solution. The simultaneous growth of NH_3 leads to a charge imbalance that needs to be rectified either by adding H^+, reducing NH_3 arbitrarily, or increasing another anion arbitrarily. Such arbitrary changes result in unreasonable aerosol compositions. Instead of balancing charge arbitrarily, gas-phase NH_3 is equilibrated with all size bins of the aerosol-phase simultaneously. This equilibration leads to exact charge balance in each bin and mass conservation of NH_3 between the gas phase and all aerosol size bins of all distributions. The equilibrium numerical solution of NH_3 between the gas phase and multiple size bins of the aerosol phase is unique in all cases, since only one gas is equilibrated. If two gases were equilibrated, the solution would not be unique when solids containing those gases were formed. The equilibration of gaseous NH_3 with the aerosol phase is, in effect, a time-dependent growth process because the amount of ammonium in the aerosol particles at a given time is tied to the growth rates of nitrate and chloride. The slower the growth rate of nitrate or chloride, the lesser the uptake of ammonium. The equilibrium treatment of NH_3 is also supported in part by *Fridlind and Jacobson* [2000] who found that, over the ocean, NH_3 be closer than HNO_3 to equilibrium with coarse-mode particles.

[22] The APNCD scheme is derived by considering the following ordinary differential equations for condensation and dissolution, respectively, from the work of *Jacobson* [1997c]:

$$\frac{dc_{q,Ni,t}}{dt} = k_{q,Ni,t-h} \left(C_{q,t} - S'_{q,Ni,t-h} C_{q,s,Ni,t-h} \right) \quad (10)$$

$$\frac{dc_{q,Ni,t}}{dt} = k_{q,Ni,t-h}\left(C_{q,t} - S'_{q,Ni,t-h}\frac{c_{q,Ni,t}}{H'_{q,Ni,t-h}}\right) \quad (11)$$

In these equations, $c_{q,Ni,t}$ is the mole concentration (mol cm^{-3}) of particle component q in size bin i of distribution N. $C_{q,t}$ is the gas-phase mole concentration (mol cm^{-3}) of component q,$C_{q,s,Ni,t-h}$ is the saturation vapor mole concentration (mol cm^{-3}) of component q over the surface of particles in size bin i of distribution N, determined at the beginning of a time step, $S'_{q,Ni,t-h}$ is the saturation ratio at equilibrium [*Jacobson*, 1999a, equation (17.45)], which accounts for the Kelvin effect, $k_{q,Ni,t-h}$ is the mass transfer rate (s^{-1}) of gas to the surface of particles in size bin i, distribution N [*Jacobson*, 1999a, equation (17.62)], and $H'_{q,Ni,t-h}$ is a dimensionless effective Henry's constant for the size bin and distribution. For HNO_3 dissolving in solution,

$$H'_{NO_3^-},Ni = R^* T\left(\frac{m_v c_{w,Ni}}{1000}\right)^2 \frac{K_{eq,HNO_3}}{c_{H^+},Ni_{\gamma^2_{Ni,H^+/NO_3^-}}} \quad (12)$$

where R^* is the universal gas constant (82.06 cm^3 atm mol^{-1} K^{-1}), T is Kelvin temperature, $K_{eq,\,HNO_3}$ is the equilibrium constant (mol^2 kg^{-2} atm^{-1}) of the reaction $HNO_3(g) \Longleftrightarrow H^+ + NO_3^-$, and γNi, H^+/NO_3^- is the dimensionless mixed activity coefficient of the ion pair H^+/NO_3^-, determined from an equilibrium calculation. A similar expression can be written for HCl dissolving in solution. Integrating equations (10) and (11) individually for one size bin over a time step h gives

$$c_q,Ni,t = c_{q,Ni,t-h} + hk_{q,Ni,t-h}(C_{q,t} - S'_{q,Ni,t-h}C_{q,s,Ni,t-h}) \quad (13)$$

$$c_{q,Ni,t} = \frac{H'_{q,Ni,t-h}C_{q,t}}{S'_{q,Ni,t-h}} + \left(c_{q,Ni,t-h} - \frac{H'_{q,Ni,t-h}c_{q,t}}{S'_{q,Ni,t-h}}\right)\exp\left(-\frac{hS'_{q,Ni,t-h}k_{q,Ni,t-h}}{H'_{q,Ni,t-h}}\right) \quad (14)$$

respectively, where the final gas mole concentration both cases, $C_{q,t}$, is currently unknown. Final aerosol and gas concentrations are constrained by the gas–aerosol mass balance equation,

$$C_{q,t} + \sum_{N=1}^{N_T}\sum_{i=1}^{N_B} c_{q,Ni,t} = C_{q,t-h} + \sum_{N=1}^{N_T}\sum_{i=1}^{N_B} c_{q,Ni,t-h} = C_{tot} \quad (15)$$

Substituting equations (13) and (14) into equation (15) and solving for $C_{q,t}$ gives a generalized solution for both condensation and dissolution,

$$C_{q,t} = \frac{C_{q,t-h} + h\sum_{N=1}^{N_T}\sum_{i=1}^{N_B}\left\{(1-D_{Ni})\left(k_{q,Ni,t-h}S'_{q,Ni,t-h}C_{q,s,Ni,t-h}\right) + D_{Ni}c_{q,Ni,t-h}\left[1-\exp\left(\frac{hS'_{q,Ni,t-h}k_{q,Ni,t-h}}{H'_{q,Ni,t-h}}\right)\right]\right\}}{1 + h\sum_{N=1}^{N_T}\sum_{i=1}^{N_B}\left\{(1-D_{Ni})k_{q,Ni,t-h} + D_{Ni}\left\{\frac{H'_{q,Ni,t-h}}{S'_{q,Ni,t-h}}\left[1-\exp\left(\frac{hS'_{q,Ni,t-h}k_{q,Ni,t-h}}{H'_{q,Ni,t-h}}\right)\right]\right\}\right\}} \quad (16)$$

where $D_{Ni} = 1$ for dissolution and 0 for condensation in the bin of the distribution. In the current application, condensation is assumed to occur for H_2O growth onto cloud drops (if the RH > 100%) and for S(VI) growth at all RHs. (At RHs < 100%, H_2O growth is by equilibrium hydration). Condensation also occurs for HNO_3 and HCl in size bins where a solid containing nitrate or chloride, respectively, forms. Solids containing nitrate include NH_4NO_3, $NaNO_3$, KNO_3, $Ca(NO_3)_2$, and $Mg(NO_4)_2$. Solids containing chloride include NH_4Cl, NaCl, KCl, $CaCl_2$, and $MgCl_2$. Dissolution occurs for HNO_3 and HCl over any size bin in which no solid containing nitrate or chloride, respectively, forms.

[23] Once equation (16) is solved for condensation, it is limited by $C_{q,t} = \min(C_{q,t},C_{tot})$, since the explicit condensation term equation (16) can result in gas concentrations in excess of the maximum gas in the system. Equation (16) cannot fall below zero in any situation, and the limit is not needed if only dissolution is considered. $C_{q,t}$ is then substituted back into equations (13) and (14) to give the final aerosol concentrations in size bins in which condensation and dissolution, respectively, occur. Whereas the dissolution solution (equation (14)) cannot result in aerosol concentrations <0 or >C_{tot}, the condensation solution (equation (13)) can. To remedy this, two limits are placed sequentially, after equations (13) and (14) are solved, when $D_{Ni} = 0$. The first is, $c_{q,Ni,t} = \mathrm{MAX}(c_{q,Ni,t}, 0)$. The second, which applies only when $c_{q,Ni,t} > c_{q,Ni,t-h}$ (and $D_{Ni} = 0$), is

$$c_{q,Ni,t} = \left\{C_{q,t-h} - C_{q,t} + \sum_{N=1}^{N_T}\sum_{i=1}^{N_B}\left\{(1-D_{Ni}) \cdot \mathrm{MAX}\left[c_{q,Ni,t-h} - c_{q,Ni,t}, 0\right] + D_{Ni}\left[c_{q,Ni,t-h} - c_{q,Ni,t}\right]\right\}\right\} \times \frac{c_{q,Ni,t} - c_{q,Ni,t-h}}{\sum_{N=1}^{N_T}\sum_{i=1}^{N_B}\left\{(1-D_{Ni})\mathrm{MAX}(c_{q,Ni,t} - c_{q,Ni,t-h}, 0)\right\}} \quad (17)$$

where the $c_{q,Ni,t}$ values on the right side of the equation are determined from equations (13) and (14). Equation (17) states that, when condensation occurs onto a particle, its concentration is set to the net loss in vapor due to condensation plus dissolution ($C_{q,t-h} - C_{q,t}$) plus the vapor gained by evaporation (from the condensation equation) minus the net change in vapor due to evaporation minus dissolution, all scaled by the rate of condensation in the bin (which equals $c_{q,Ni,t} - c_{q,Ni,t-h}$ from equation (13)) divided by the sum of the rates of condensation into all bins in which condensation occurs. No limit is needed if only dissolution is considered. Thus, the solution scheme in equations (13)–(17) is exactly mass conserving between the gas and aerosol phases under all conditions and is noniterative. The solution scheme is also unconditionally stable because the difference between the numerical and exact solution is bounded between 0 and C_{tot}, regardless of the time step or integration time.

[24] When HNO_3 or HCl grows onto a size bin and a solid exists in the bin, condensational growth terms are needed in equations (13)–(17). Such terms require a saturation vapor mole concentration. For HNO_3, the SVMC is calculated as

$$c_{\mathrm{HNO_3},s,Ni} = \min \left\{ \begin{array}{l} \dfrac{c_{\mathrm{NO_3^-},Ni}}{H'_{\mathrm{NO_3^-}}} = \dfrac{1}{R^*T}\left(\dfrac{1000}{m_v c_{w,Ni}}\right)^2 \dfrac{c_{\mathrm{H^+},Ni} c_{\mathrm{NO_3^-},Ni} \gamma^2_{Ni,\mathrm{H^+/NO_3^-}}}{K_{eq,\mathrm{HNO_3}}} \\ \left(\dfrac{1}{R^*T}\right)^2 \dfrac{K_{s,\mathrm{NH_4NO_3}}}{C_{\mathrm{NH_3}}}, \\ \dfrac{1}{R^*T} \dfrac{c_{\mathrm{H^+},Ni}\gamma^2_{Ni,\mathrm{H^+/NO_3^-}}}{K_{eq,\mathrm{HNO_3}}} \dfrac{K_{eq,\mathrm{NH_4NO_3}}}{c_{\mathrm{NH_4^+},Ni}\gamma^2_{Ni,\mathrm{NH_4^+/NO_3^-}}} \\ \dfrac{1}{R^*T} \dfrac{c_{\mathrm{H^+},Ni}\gamma^2_{Ni,\mathrm{H^+/NO_3^-}}}{K_{eq,\mathrm{HNO_3}}} \dfrac{K_{eq,\mathrm{NaNO_3}}}{c_{\mathrm{Na^+},Ni}\gamma^2_{Ni,\mathrm{Na^+/NO_3^-}}}, \\ \dfrac{1}{R^*T} \dfrac{c_{\mathrm{H^+},Ni}\gamma^2_{Ni,\mathrm{H^+/NO_3^-}}}{K_{eq,\mathrm{HNO_3}}} \dfrac{K_{eq,\mathrm{KNO_3}}}{c_{\mathrm{K^+},Ni}\gamma^2_{Ni,\mathrm{K^+/NO_3^-}}}, \\ \dfrac{1}{R^*T} \dfrac{c_{\mathrm{H^+},Ni}\gamma^2_{Ni,\mathrm{H^+/NO_3^-}}}{K_{eq,\mathrm{HNO_3}}} \sqrt{\dfrac{1000}{m_v c_{w,Ni}} \dfrac{K_{eq,\mathrm{Ca(NO_3)_2}}}{c_{\mathrm{Ca^2},Ni}\gamma^3_{Ni,\mathrm{Ca^{2+}/NO_3^-}}}}, \\ \dfrac{1}{R^*T} \dfrac{c_{\mathrm{H^+},Ni}\gamma^2_{Ni,\mathrm{H^+/NO_3^-}}}{K_{eq,\mathrm{HNO_3}}} \sqrt{\dfrac{1000}{m_v c_{w,Ni}} \dfrac{K_{eq,\mathrm{Mg(NO_3)_2}}}{c_{\mathrm{Mg^{2+}},Ni}\gamma^3_{Ni,\mathrm{Mg^{2+}/NO_3^-}}}}, \end{array} \right\} \quad (18)$$

which states that the SVMC is the minimum SVMC arising from several processes. All terms in equation (18) are evaluated at the beginning of a growth time step. The use of equation (18) allows more nitrate mass to transfer to the aerosol phase when a solid is present than the APD scheme originally allowed when only solubility was considered. The first process in equation (18) is dissolution by the reaction,

$$\mathrm{HNO_3(g) = H^+ + NO_3^-} \quad (19)$$

which has the equilibrium coefficient expression,

$$\left(\frac{1000}{m_v c_{w,Ni}}\right)^2 \frac{c^+_{\mathrm{H},Ni} c_{\mathrm{NO_3^-},Ni}}{C_{\mathrm{HNO_3},s,Ni} R^* T} \cdot \gamma^2_{Ni,\mathrm{H^+/NO_3^-}} = K_{eq,\mathrm{HNO_3}} \left(\frac{\mathrm{mol^2}}{\mathrm{kg^2 - atm}}\right) \quad (20)$$

Solving equation (20) for $C_{\mathrm{HNO_3},s,Ni}$ gives the SVMC term in equation (18). The second process is the solid–gas reaction

$$\mathrm{NH_4NO_3(s) = NH_3(g) + HNO_3(g)} \quad (21)$$

which has an equilibrium coefficient expression,

$$\left(R^* T\right)^2 c_{\mathrm{NH_3},Ni} C_{\mathrm{HNO_3}} = K_{s,\mathrm{NH_4NO_3}} \left(\mathrm{atm^2}\right) \quad (22)$$

All remaining processes are solid–ion reactions coupled with the gas–ion reaction $\mathrm{HNO_3(g) = H^+ + NO_3^-}$. The five solid–ion reactions are

$$\mathrm{NH_4NO_3(s) = NH_4^+ + NO_3^-} \quad (23)$$

$$\mathrm{NaNO_3(s) = Na^+ + NO_3^-} \quad (24)$$

$$\mathrm{KNO_3(s) = K^+ + NO_3^-} \quad (25)$$

$$\mathrm{Ca(NO_3)_2(s) = Ca^{2+} + 2NO_3^-} \quad (26)$$

$$\mathrm{Mg(NO_3)_2(s) = Mg^{2+} + 2NO_3^-} \quad (27)$$

The corresponding equilibrium coefficient expressions for these reactions are

$$\left(\frac{1000}{m_v c_{w,Ni}}\right)^2 c^+_{\mathrm{NH_4},Ni}\, c_{\mathrm{NO_3^-},Ni}\gamma^2_{Ni,\mathrm{NH_4^+/NO_3^-}} = K_{eq,\mathrm{NH_4NO_3}} \left(\frac{\mathrm{mol^2}}{\mathrm{kg^2}}\right) \quad (28)$$

$$\left(\frac{1000}{m_v c_{w,Ni}}\right)^2 c^+_{\mathrm{Na},Ni}\, c^2_{\mathrm{NO_3^-},Ni}\gamma^2_{Ni,\mathrm{Na^+/NO_3^-}} = K_{eq,\mathrm{NaNO_3}} \left(\frac{\mathrm{mol^2}}{\mathrm{kg^2}}\right) \quad (29)$$

$$\left(\frac{1000}{m_v c_{w,Ni}}\right)^2 c^+_{\mathrm{K},Ni}\, c_{\mathrm{NO_3^-},Ni}\gamma_{Ni,\mathrm{K+/NO_3^{-2}}} = K_{eq,\mathrm{KNO_3}} \left(\frac{\mathrm{mol^2}}{\mathrm{kg^2}}\right) \quad (30)$$

$$\left(\frac{1000}{m_v c_{w,Ni}}\right)^3 c_{\mathrm{Ca^{2+}},Ni}\, c^2_{\mathrm{NO_3^-},Ni}\gamma_{Ni,\mathrm{Ca^{2+}/NO_3{}^3}} = K_{eq,\mathrm{Ca(NO_3)_2}} \left(\frac{\mathrm{mol^3}}{\mathrm{kg^3}}\right) \quad (31)$$

$$\left(\frac{1000}{m_v c_{w,Ni}}\right)^3 c_{\mathrm{Mg^{2+}},Ni}\, c^2_{\mathrm{NO_3^-},Ni}\gamma_{Ni,\mathrm{Mg^{2+}/NO_3{}^3}} = K_{eq,\mathrm{Mg(NO_3)_2}} \left(\frac{\mathrm{mol^3}}{\mathrm{kg^3}}\right) \quad (32)$$

respectively. Coupling these equations with equation (20) and solving for $C_{\mathrm{HNO_3},s,Ni}$ gives the SVMC terms in equation (18). The SVMCs for HCl are calculated in a similar way.

[25] When homogeneous nucleation is coupled with growth, such as in the case of binary homogeneous nucleation/condensation of S(VI), the nucleation rate is first converted to a mass transfer rate between the gas and aerosol and added to the growth mass transfer rate in the first size bin. For example, if the binary homogeneous nucleation rate of S(VI)–water particles is $R_{\mathrm{S(VI)-H_2O}}$ (new particles per cubic centimeter per second), and if this quantity exceeds zero (and if the initial partial pressure of S(VI), $C_{\mathrm{S(VI)},t-h}$, exceeds $S'_{\mathrm{S(VI)},N1,t-h} C_{\mathrm{S(VI)},s,N1,t-h}$), $R_{\mathrm{S(VI)-H_2O}}$ is converted to a gas-phase mass transfer rate for nucleation ($\mathrm{s^{-1}}$) with

$$k_{\mathrm{S(VI),\,nuc},N1,t-h} = R_{\mathrm{S(VI)-H_2O}} \frac{\rho_{\mathrm{S(VI)}} \upsilon_{N1} F_{\mathrm{S(VI)}}}{m_{\mathrm{S(VI)}}} \cdot \left(\frac{1}{C_{\mathrm{S(VI)},t-h} - S'_{\mathrm{S(VI)},N1,t-h} C_{\mathrm{S(VI)},s,N1,t-h}}\right) \quad (33)$$

where $\rho_{\mathrm{S(VI)}}$ is the density of pure S(VI) (g $\mathrm{cm^{-3}}$), υ_{N1} is the single-particle volume of a nucleated particle (cubic centimeters per particle), $F_{\mathrm{S(VI)}}$ is the volume fraction of S(VI) in an S(VI)–H_2O nucleated mixture, and $m_{\mathrm{S(VI)}}$ is the molecular weight (grams per mole) of S(VI). The denominator on the right side of equation (33) is the maximum gas

available for nucleation at the beginning of the time step (mol cm^{-3}). The mass transfer rate in equation (33) is then added to the growth mass transfer rate ($k_{S(VI),grow,N1,t-h}$) for the size bin in which nucleated particles are placed (assumed to be bin 1 in this equation), to give a total mass transfer rate to this bin of $k_{S(VI),N1,t-h} = k_{S(VI),grow,N1,t-h} + k_{S(VI),nuc,N1,t-h}$.

[26] After equations (13)–(17) are solved with the revised growth plus nucleation transfer rate, the new number concentration of S(VI)–H_2O particles due to homogeneous nucleation is calculated from the incremental change in mole concentration of S(VI) with

$$n_{N1,t} = n_{N1,t-h} + \mathrm{MAX}\left[\left(c_{S(VI),N1,t} - c_{S(VI),N1,t-h}\right)\frac{m_{S(VI)}}{\rho_{S(VI)}\upsilon_{N1}F_{S(VI)}}\frac{k_{S(VI),nuc,N1,t-h}}{k_{S(VI),N1,t-h}}, 0\right] \quad (34)$$

Once new particles are added, water, with a volume fraction of $1 - F_{S(VI)}$, is added to ensure the total volume added to the size distribution is consistent with the number of particles added to the distribution. This water content and the single-particle volume are adjusted subsequently when equilibrium hydration equations are solved.

[27] The advantage of coupling nucleation with growth is that rates for both are fast, and if these processes are operator split, one process will be favored extensively over the other. Solving both processes together allows for a more realistic competition among size bins for the limited amount of sulfuric acid gas available for nucleation and condensation.

[28] The nucleation rate, $R_{S(VI)-H_2O}$, is calculated with classical theory in the simulations discussed below but could also be calculated with a parameterization. *Zhang et al.* [1999] compare several parameterizations of nucleation rates.

5. Aerosol Optical Properties

[29] Aerosol optical depths, single-scattering albedos, and asymmetry parameters are determined from particle scattering, absorption, and forward-scattering efficiencies from Mie theory calculations under the assumption that when a particle contains BC, BC is core material and all other material is shell material. Shell real and imaginary refractive indices for a given particle size and wavelength are obtained by first calculating solution and nonsolution refractive indices of all non-BC substances in the shell, then volume averaging the solution and nonsolution refractive indices to obtain average shell refractive indices. These refractive indices are then used in a core-shell Mie theory calculation in which BC is core [e.g., *Toon and Ackerman*, 1981].

[30] The volume-averaged shell real and imaginary refractive indices for a given wavelength λ and particle size i in distribution N are calculated as

$$\mathrm{n}_{shell,Ni,\lambda} = \left(v_{s,Ni}\mathrm{n}_{s,Ni,\lambda} + \sum_{\substack{q=1\\q\neq BC}}^{N_{NS}} v_{q,Ni}\mathrm{n}_{q,\lambda}\right) \Bigg/ \left(v_{s,i} + \sum_{\substack{q=1\\q\neq BC}}^{N_{NS}} v_{q,Ni}\right) \quad (35)$$

$$\kappa_{shell,Ni,\lambda} = \left(v_{s,Ni}\kappa_{s,Ni,\lambda} + \sum_{\substack{q=1\\q\neq BC}}^{N_{NS}} v_{q,Ni}\kappa_{q,\lambda}\right) \Bigg/ \left(v_{s,Ni} + \sum_{\substack{q=1\\q\neq BC}}^{N_{NS}} v_{q,Ni}\right) \quad (36)$$

where $\mathrm{n}_{s,Ni,\lambda}$ and $\mathrm{n}_{q,\lambda}$ are the overall solution and individual component nonsolution real refractive indices, respectively, and $\kappa_{s,Ni,\lambda}$ and $\kappa_{q,\lambda}$ are overall solution and individual component nonsolution imaginary refractive indices. The solution real refractive index is

$$\mathrm{n}_{s,Ni,\lambda} = \sqrt{\frac{v_{s,Ni} + 2R_{s,Ni,\lambda}c_{s,Ni}}{v_{s,Ni} - R_{s,Ni,\lambda}c_{s,Ni}}} \quad (37)$$

derived from equation (1) of *Stelson* [1990], where

$$R_{s,Ni,\lambda}c_{s,Ni} = R_{H_2O,\lambda}c_{H_2O}, Ni + \sum_{q=1}^{N_S} R_{q,\lambda}c_{q,Ni} \quad (38)$$

is the product of the molar refraction ($R_{s,Ni,\lambda}$, $cm^3\ mol^{-1}$) and mole concentration ($c_{s,Ni}$, mol cm^{-3}) of the solution, and $R_{q,\lambda}$ is the partial molar refraction ($cm^3\ mol^{-1}$) of individual solution component q (either ion or electrolyte). Partial molar refractions are given for several ions and aqueous electrolytes in the works of *Stelson* [1990] and *Tang* [1997] at 550 nm. When data are not available, such as at solar- and thermal-IR wavelengths and for certain species, partial molar refractions for aqueous electrolytes are estimated by combining all ions in solution into hypothetical aqueous electrolytes, assuming the refractive index of the aqueous electrolyte equals that of the corresponding solid electrolyte, and applying the equation,

$$R_{q,\lambda} = \frac{m_q}{\rho_q}\left(\frac{n_{q,n}^2 - 1}{n_{q,n}^2 + 2}\right) \quad (39)$$

where $\mathrm{n}_{q,\lambda}$ is the real refractive index, m_q is the molecular weight (g mol^{-1}), and ρ_q is the density (g cm^{-3}) of the solid electrolyte. The assumption that the partial molar refraction of an aqueous electrolyte is similar to that of the corresponding solid electrolyte is substantiated by the work of *Stelson* [1990, Figure 1].

[31] The solution imaginary refractive index is estimated here with

$$\kappa_{s,Ni,\lambda} = \frac{A_{s,Ni,\lambda}c_{s,Ni}}{v_{s,Ni}} \quad (40)$$

where

$$A_{s,Ni,\lambda}c_{s,Ni} = A_{H_2O,\lambda}c_{H_2O,Ni} + \sum_{q=1}^{N_S} A_{q,\lambda}c_{q,Ni} \quad (41)$$

is the product of the molar absorption ($A_{s,Ni,\lambda}$, $cm^3\ mol^{-1}$) and the mole concentration of the solution, and $A_{q,\lambda}$ is the partial molar absorption ($cm^3\ mol^{-1}$) of individual solution component (either ion or electrolyte) q. Since partial molar absorption data of ions and aqueous electrolytes are

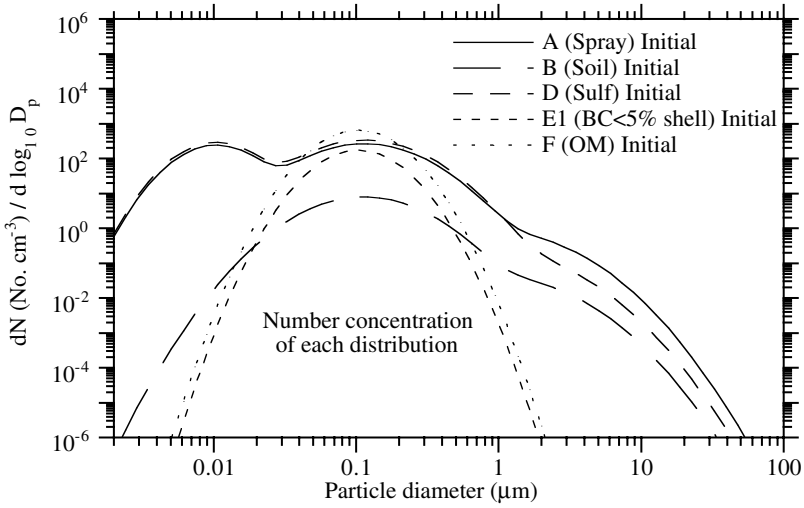

Figure 1. Initial number concentrations of five externally mixed size distributions used for all simulations.

unavailable, such quantities are estimated by combining all ions in solution into hypothetical electrolytes, assuming the partial molar absorptions of aqueous electrolytes equal those of solid electrolytes, then applying the equation,

$$A_{q,\lambda} = \frac{m_q}{\rho_q} \kappa_{q,\lambda} \tag{42}$$

where $\kappa_{q,\lambda}$ is the imaginary refractive index of solid electrolyte q. Equations (40)–(42) result in a imaginary index mixing rule for aerosol solutions that is analogous to a volume-averaged mixing rule, except that here, the imaginary index is scaled by the ratio of the solution density to the weighted sum of the densities of the individual electrolytes and water in solution. Sources of wavelength-dependent imaginary refractive indices for some species treated here include the following: liquid water [*Hale and Querry*, 1973], organic compounds and black carbon [*Krekov*, 1993], organic compounds and ammonium nitrate in the UV [*Jacobson*, 1999c], sodium chloride and ammonium sulfate [*Toon et al.*, 1976], calcium sulfate and potassium chloride [*Query*, 1987], and sulfuric acid [*Palmer and Williams*, 1975].

6. 0-D Simulations of the Aerosol/Radiative Algorithms

[32] Here, the processes described above are analyzed in 0-D case studies. In all cases, except for one, the simulations were run with the moving-center size structure. In all cases, the distributions and species considered were those in Tables 1a and 1b. In all cases, five distributions (A, B, D, E1, and F) were initialized. Except where specified, the RH was 90% and the temperature was T = 285 K. Initial distributions are shown in Figure 1. The initial number and mass concentrations, summed over each distribution, were as follows: A, sea spray: 502 cm^{-3}, 54.6 μg m^{-3} (84% of which was water); B, soil: 6.1 cm^{-3}; 0.72 μg m^{-3}; C, sulfate: 1192 cm^{-3}; 11.2 μg m^{-3} (82% of which was water); E1, BC < 5% shell: 90 cm^{-3}, 0.25 μg m^{-3}; F, primary organic matter (OM): 337 cm^{-3}, 0.75 μg m^{-3}. These initial conditions represent sea spray particles interacting with low to moderate loadings of soil, sulfate, BC, and OM at a high RH. The initial number and mass concentrations, summed over all distributions, were 2127 cm^{-3} and 67.5 μg m^{-3} (82% of which was water), respectively.

6.1. Coagulation Alone

[33] In the first simulation, coagulation alone was simulated for a 12 hour period among the five externally mixed distributions A, B, D, E1, and F to produce larger particles in the same distributions, all possible binary mixtures of distributions (e.g., AB, AD, AE, . . .), and higher mixtures (MX). Distributions E2 and E3 were not needed in this simulation, since no growth onto E1 particles was considered.

[34] Figure 2a compares the initial and final particle number concentrations, summed over all distributions, resulting from the simulation. The figure appears to indicate, as past coagulation simulations of one size distribution have indicated [e.g., *Jacobson*, 1997a, Figures 2 and 3], that coagulation among multiple distributions has little effect on the total number concentration of particles larger than 0.2 μm in diameter over a 12 hour period. Figure 2b clarifies this misconception. It shows that coagulation among multiple distributions internally mixes particles of different original compositions, affecting the composition of the entire size distribution without affecting the number concentration of large particles summed over all distributions.

[35] The results shown in Figure 2b suggest that in an air mass containing a moderate loading of particulates, coagu-

Figure 2. (opposite) Coagulation alone. Results of simulation in which the five externally mixed distributions from Figure 1 were coagulated over 12 hours to produce 16 externally and internally mixed distributions. (a) The initial and final number concentrations summed over all distributions. (b) The final number concentrations by distribution. (c–e) The initial and final mass concentrations of (c) S(VI), (d) BC, and (e) soil in each distribution. S(VI) = H_2SO_4 (aq) + HSO_4^- + SO_4^{2-}.

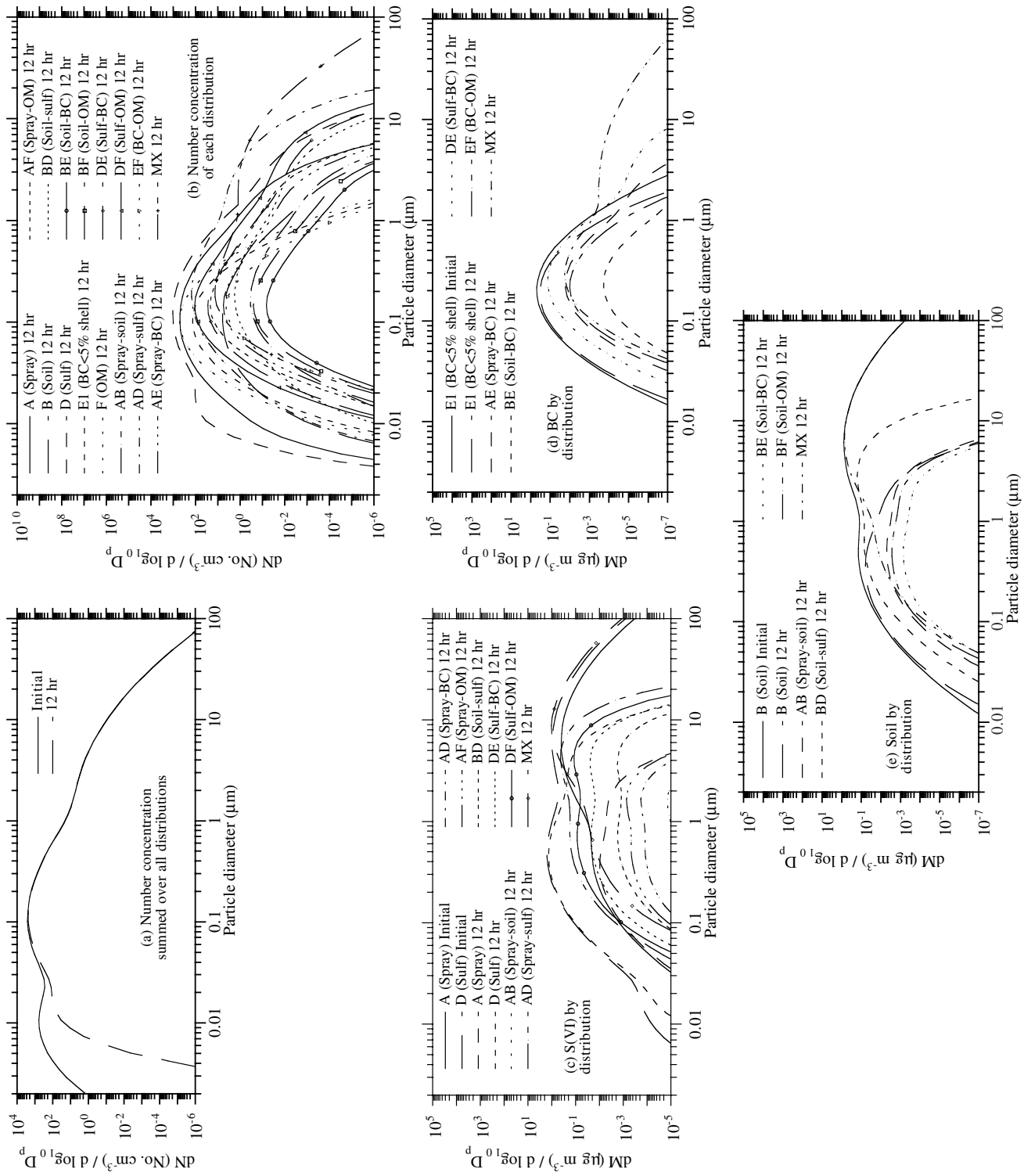
(a) Number concentration summed over all distributions
Initial
12 hr
dN (No. cm-3) / d log10 Dp
Particle diameter (μm)
(b) Number concentration of each distribution
A (Spray) 12 hr
B (Soil) 12 hr
D (Sulf) 12 hr
E1 (BC<5% shell) 12 hr
F (OM) 12 hr
AB (Spray-soil) 12 hr
AD (Spray-sulf) 12 hr
AE (Spray-BC) 12 hr
AF (Spray-OM) 12 hr
BD (Soil-sulf) 12 hr
BE (Soil-BC) 12 hr
BF (Soil-OM) 12 hr
DE (Sulf-BC) 12 hr
DF (Sulf-OM) 12 hr
EF (BC-OM) 12 hr
MX 12 hr
(c) S(VI) by distribution
A (Spray) Initial
D (Sulf) Initial
dM (μg m-3) / d log10 Dp
(d) BC by distribution
E1 (BC<5% shell) Initial
(e) Soil by distribution
B (Soil) Initial

lation alone can internally mix most particles to some degree within 12 hours. In the simulation, coagulation internally mixed almost all the largest particles and a smaller percent of the smaller particles, which may explain a result of *Okada and Hitzenberger* [2001], who found that the number fraction of mixed particles in Vienna increased with increasing particle radius and with increasing particle abundance.

[36] Not only did coagulation cause a greater fraction of larger particles than smaller particles to mix internally, but it also caused mixtures of larger particles to obtain more components than mixtures of smaller particles. Since the combination of even the smallest with the largest particle is considered a mixture, though, an internally mixed large particle can often contain a trivial amount of a second and/or third component.

[37] Of the total reduction in particle number concentration during the 12 hour simulation, an estimated 97.283% was due to Brownian motion, 2.716% was due to Brownian convective diffusion enhancement, 0.000984% was due to turbulent inertial motion plus turbulent shear, and 0.000089% was due to gravitational collection. Aside from Brownian motion, convective diffusion enhancement had the greatest effect on coagulating small particles with large particles.

[38] Figures 2c–2e show the fate of S(VI), BC, and soil mass concentration by distribution resulting from the simulation. Because S(VI) was initially in two distributions (A and D) whereas BC and soil were initially in one, coagulation spread S(VI) among more distributions than it spread the other components. Figure 2d shows that, although BC did not exist in large particles initially, coagulation of BC with large particles from other distributions put BC into such particles. Most of the largest particles that BC entered contained components from at least two other distributions to form mixed (MX) particles. Figure 2e shows that most large soil particles, which existed initially, coagulated with (most likely) small particles from at least two other distributions to form mixed particles.

6.2. Nucleation and Condensation Alone

[39] Figure 3 shows results when condensation of 1 $\mu g\ m^{-3}$ of gas-phase S(VI) (as sulfuric acid) was grown simultaneously onto the five particle size distributions initialized in Figure 1. Homogeneous nucleation of S(VI) was solved simultaneously in distribution D. All nucleated particles were assumed to enter a bin the size of their critical radius and to grow in competition with other particles. Coagulation was ignored in this simulation. The RH was 90% and the temperature was 285 K.

[40] Figures 3a and 3b show that nucleation and growth modified the number and mass concentrations of the sulfate distribution (D) the most. Including nucleation in this case allowed the production of 1.2×10^5 new particles per cubic centimeter during the 12 hour simulation. In the absence of competitive growth, homogeneous nucleation of 1 $\mu g\ m^{-3}$ of S(VI) would have produced over 1×10^8 particles cm^{-3} at the critical radius, so solving growth simultaneously with nucleation and conserving mass between the gas and aerosol phases curtailed the runaway particle production that would have been predicted if an explicit calculation were performed. Homogeneous nucleation was not swamped out by growth during the simulation because the initial number concentration of all particles together was not large (2127 particles cm^{-3}). Doubling the initial number of particles decreased the number of nucleated particles by more than one half. Thus, as the number concentration of existing particles increased, the more condensation of S(VI) was favored over homogeneous nucleation. Although most new sulfuric acid water particles formed at a diameter near 0.002 μm, condensation onto these particles caused them to grow to around 0.008 μm, as illustrated in Figures 3a and 3b.

[41] Figure 3c shows that growth of S(VI) caused most small BC particles to obtain a shell >20% by volume and most midsize BC particles to obtain a shell 5–20% by volume after 12 hours. Only larger BC particles avoided significant growth of S(VI). This result suggests that condensation increases the fractional coating of small particles more than large particles. Condensation similarly affected primarily small OM particles (Figure 3a), soil particles (Figures 3a and 3d), and sea spray particles (Figure 3a).

6.3. Nucleation, Condensation, and Coagulation

[42] Figure 4 shows results when coagulation was added to the simulation of Figure 3, which accounted for homogeneous nucleation and condensation of S(VI). Figure 4a shows that coagulation reduced the distinct nucleation-mode number concentration peak, obtained when coagulation was ignored, by a factor of 40 over the 12 hour period, from 1.2×10^5 particles cm^{-3} in Figure 3 to 3000 particles cm^{-3} in Figure 4. At the same time, coagulation reduced the number concentration of particles >0.3 μm in diameter by only 12%, from 86 to 76 particles cm^{-3}.

[43] The large reduction in sulfate particle number concentration when coagulation was included versus when it was not suggests that heterocoagulation during S(VI) nucleation might have caused significant internal mixing of sulfate with other distributions. This can be verified by comparing Figure 4 with Figure 2 (the coagulation-only case). Whereas coagulation alone permitted a large number of BC and soil particles to remain externally mixed (Figures 2c and 2d), coagulation of newly nucleated S(VI) particles internally mixed almost all BC and soil particles (Figures 4c and 4d), producing sulfate–BC particles (DE), soil–sulfate particles (BD), and higher mixtures (MX). This internal mixing was due primarily to coagulation rather than growth because the only source of BD, DE, and MX particles is coagulation. Growth of S(VI) onto primary BC particles (E1) produces E2 and E3 particles. E1, E2, and E3 particles all coagulate with S(VI) (distribution D) to form DE particles. Since the concentrations of E1, E2, and E3 particles were negligible at the end of this simulation, internal mixing of BC must have been due primarily to coagulation, although some of it was due to growth that created E2 and E3 particles, which subsequently coagulated.

6.4. Nucleation, Condensation, and Dissolution/Chemistry

[44] Figure 5 shows results when homogeneous nucleation and condensation of S(VI), dissolution of HCl, HNO_3, and NH_3, internal particle chemical equilibrium and equilibrium hydration were solved between the gas phase and all particle size distributions. The initial concentrations of gas-phase S(VI), HCl, HNO_3, and NH_3 were 1, 0, 0.8, and 0.3 $\mu g\ m^{-3}$, respectively. The RH was 90%, and T = 285 K. Simulations with each the moving-center and full-moving

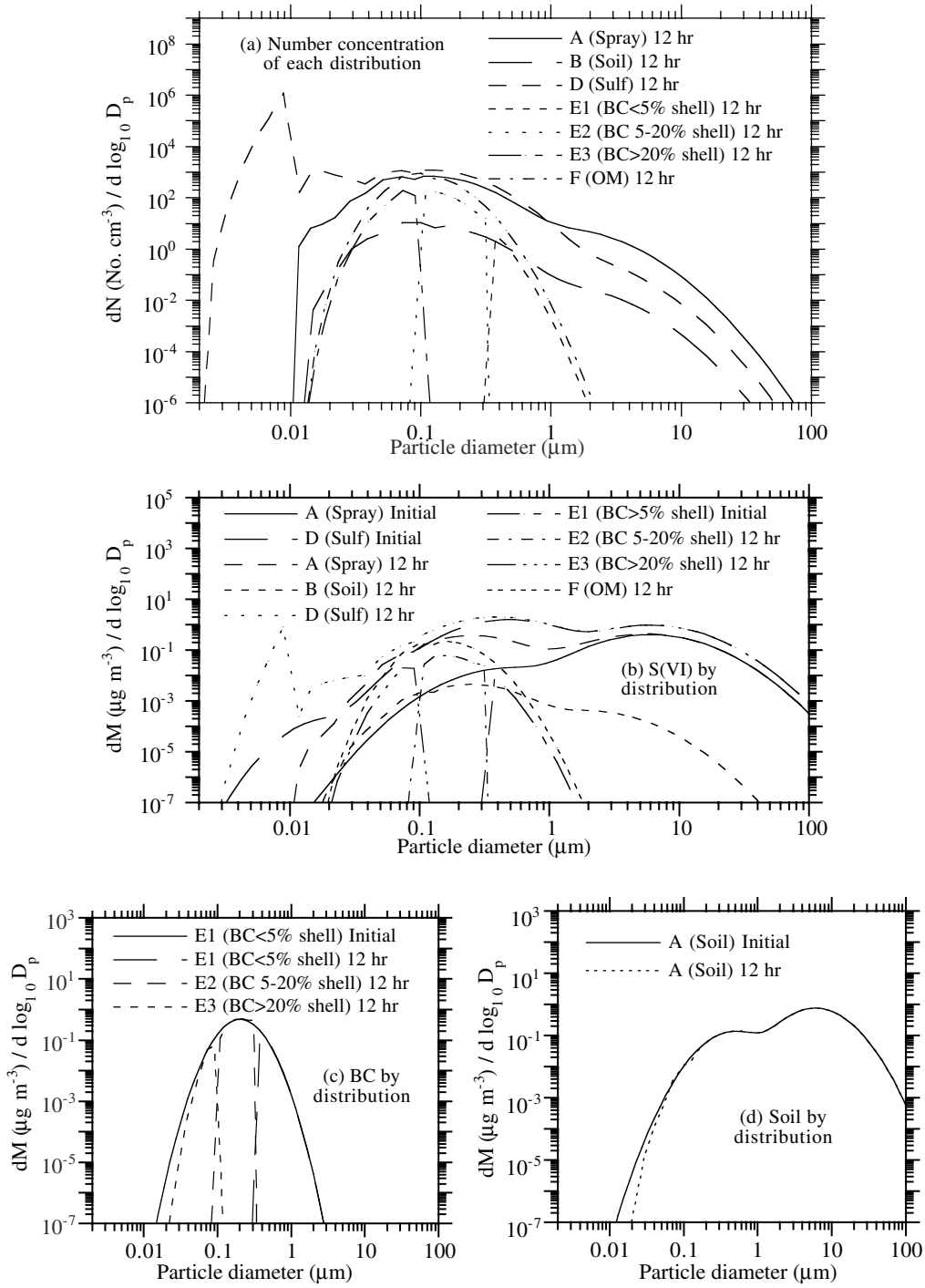

Figure 3. Nucleation and condensation alone. (a) Number concentrations of seven size distributions after 12 hours of nucleation and condensation of S(VI) onto the five distributions shown in Figure 1. The two extra distributions, E2 and E3, resulted by growing S(VI) onto distribution E1, as described in the text. Condensation was solved among all seven distributions and the gas phase. Nucleation was solved simultaneously, but only between the gas phase and distribution D. The initial gas-phase concentration of S(VI) was 1 $\mu g\ m^{-3}$, and the RH was 90%. (b–d) The initial and final mass concentrations of (b) S(VI), (c) BC, and (d) soil in each distribution.

size structures were run. Coagulation was not solved in this case.

[45] Figures 5a.i and 5b show that, in comparison with Figure 3, accounting for additional growth processes caused the newly nucleated S(VI) and other particles to grow to larger sizes than when these processes were ignored. Dissolutional growth and hydration also caused BC particles to obtain larger shell fractions and grow to slightly larger sizes

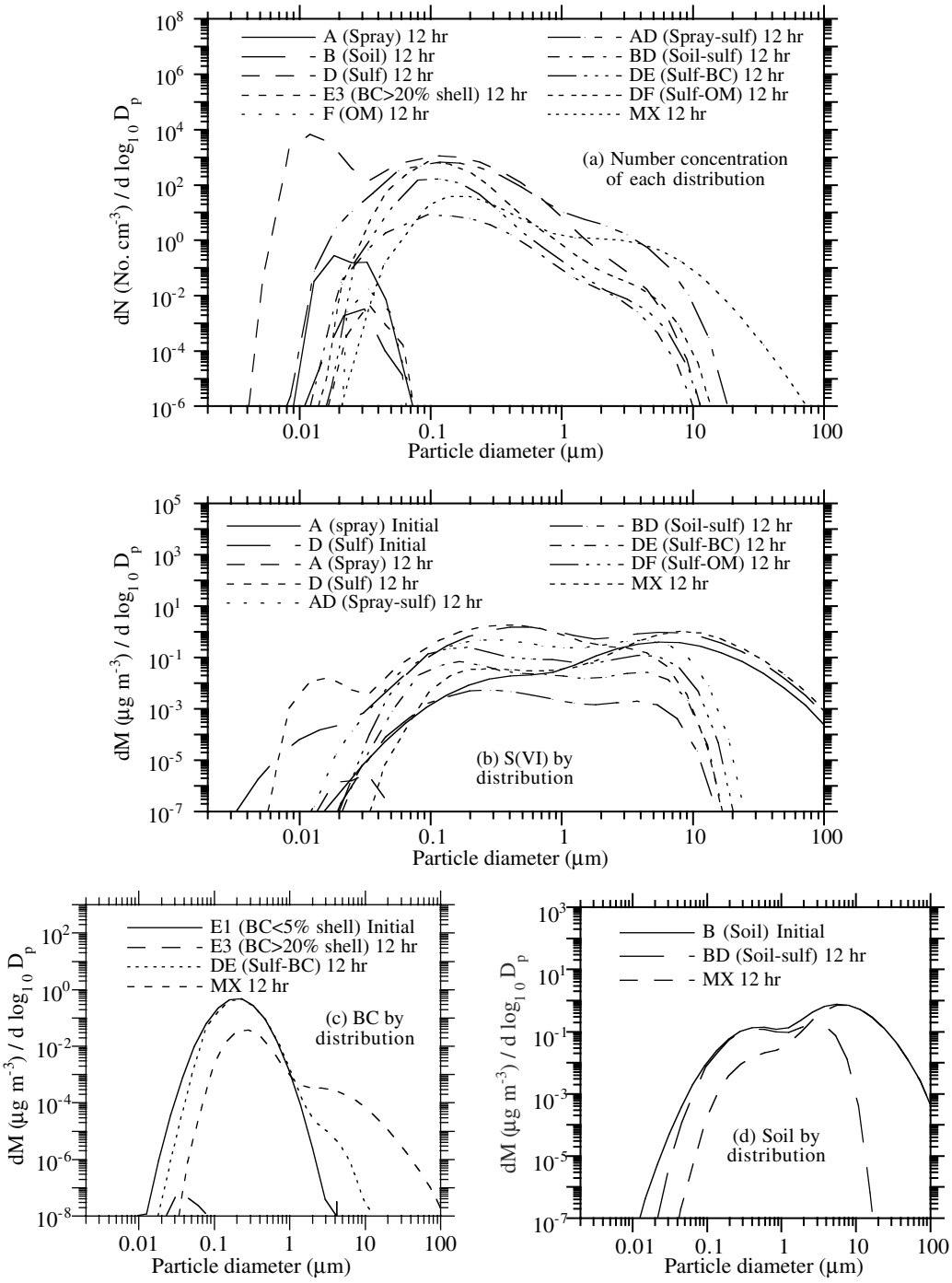

Figure 4. Nucleation, coagulation, and condensation. Same as Figure 3, but when coagulation was treated as well (thus, more distributions were affected).

(Figure 5c versus Figure 3c). Soil similarly grew to larger sizes (Figure 5d versus Figure 3d).

[46] Figure 5e shows the fate of liquid water by distribution. Water uptake was due solely to equilibrium hydration, thus the presence of water in a distribution indicated the distribution contained hygroscopic material by the end of the simulation. Initially, BC, OM, and soil distributions did not contain hygroscopic material. These distributions obtained such material only after S(VI) condensed on them, simultaneously hydrating liquid water. Once liquid water was present, HCl, NH_3, and HNO_3 could dissolve, changing the solution pH and hydrating more water. Figures 3b and 5b show that S(VI) condensed on the BC, OM, and soil distributions. Figures 5f–5h show that HCl, NH_3, and HNO_3, respectively, dissolved in the resulting S(VI)–H_2O solution. Since no HCl gas existed initially, all the chloride in distributions aside from the sea spray distribution (A) must have evaporated from that distribution to the gas phase then dissolved in the other distributions. Indeed, Figure 5f shows that chloride was lost primarily from small particles in the sea spray distribution (A). This resulted from acidification of the small sea spray particles by sulfate and

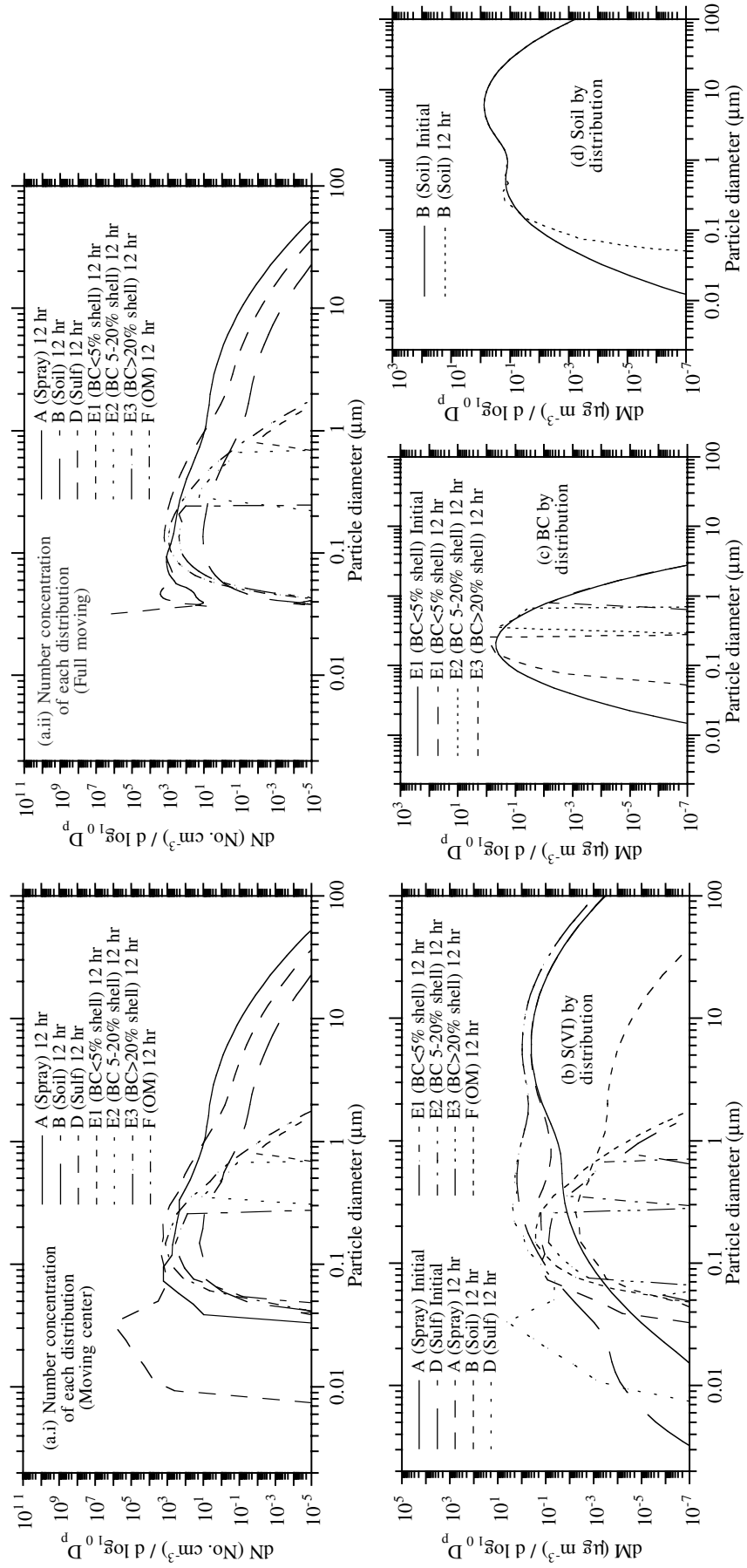

Figure 5. Nucleation, condensation, and dissolution/equilibrium. (a.i) Number concentrations of seven distributions after 12 hours of nucleation and condensation of S(VI), dissolution of HCl, HNO_3, NH_3, internal particle equilibrium, and equilibrium hydration. The initial gas concentrations of S(VI), HCl, HNO_3, and NH_3 were 1, 0, 0.8, and 0.3 μg m^{-3}, respectively, and the RH was 90%. Condensation was solved among all distributions and the gas phase. Nucleation was solved simultaneously with condensation over distribution D. The moving-center size structure was used. (a.ii) Same as (a.i), except the full-moving size structure was used (all nucleated material was placed in the smallest current bin in that case). (b–h) Initial and final mass concentration of (b) S(VI), (c) BC, (d) soil, (e) H_2O(l), (f) Cl^-, (g) NH_4^+, and (h) NO_3^- in each distribution, all obtained when the moving-center structure was used.

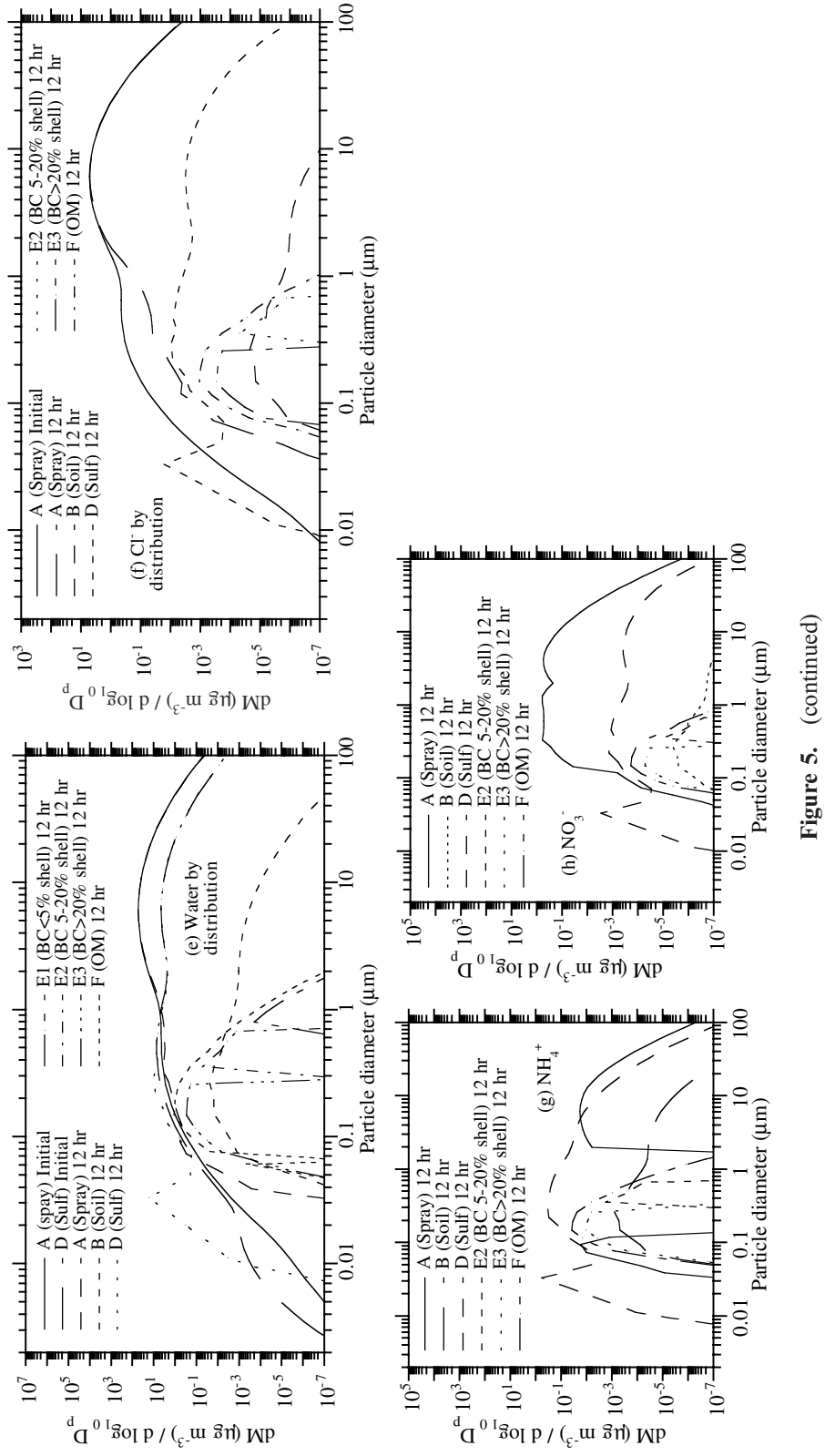

Figure 5. (continued)

nitrate, as shown in Figures 5b and 5h, respectively. The growth of sulfate and nitrate onto the smallest sea spray particles simultaneously increased the size of these particles (Figure 5a.i) so that the smallest sea spray particles not only grew, but they also lost their chloride.

[47] Figure 5g shows that ammonium entered both small and large sea spray particles but not particles between around 0.15 and 1.5 μm. Ammonium entered the small particles to balance sulfate and other anions in excess of Na^+, Ca^{2+}, Mg^{2+}, and K^+. It entered the large particles to balance the nitrate and other anions in excess of these cations. Sulfate and nitrate both entered 0.15–1.5 μm particles, joining chloride there, but these anions were balanced there by the cations, preventing the dissolution of ammonia.

[48] Figure 5a.ii shows the final number concentration distribution for the simulation shown in Figure 5a.i, but when the full-moving size structure was used. The comparison between the full-moving and moving-center structures was done because the full-moving structure allows zero diffusion during growth. However, a problem with the full-moving structure, illustrated here, is that, once growth increases the size of the smallest size bin, no real bin exists for nucleation to occur within. Since the simulation here included nucleation, all nucleated particles were placed in the smallest full-moving bin, which was much larger than the critical radius for nucleation (except at the beginning of the simulation). In the moving-center structure, a small bin always exists for nucleation. Thus, the apparent difference in results in the nucleation mode between the two simulations is due substantially to the inability to treat nucleation physically in the full-moving structure. The rest of the size distribution in both structures are nearly identical, indicating that the moving-center structure was non-diffusive yet also treated nucleation physically.

6.5. Nucleation, Condensation, Coagulation, and Dissolution/Chemistry

[49] Figure 6 shows results when coagulation was added to the moving-center simulation at 90% RH shown in Figure 5. Thus, the simulation included nucleation, condensation, dissolution, equilibrium chemistry, equilibrium hydration, and coagulation. A comparison of Figure 6a with Figure 5a suggests that coagulation reduced the number of nucleated S(VI) particles, as it did when dissolution was ignored. This simulation also reaffirms that coagulation internally mixes a greater fraction of larger particles than smaller particles and leaves only a residual of externally mixed small particles unaffected when new sources of those particles are not considered. After 12 hours, most initial externally mixed particles from the simulation were internally mixed with one or more distributions. The sulfate distribution, which had a new-particle source during the simulation, remained more externally mixed than did other distributions, which did not have new-particle sources. Figure 6b shows that although a good portion of sulfate remained externally mixed, a large fraction became internally mixed during the simulation.

[50] Figure 6c shows that only a small amount of BC remained uncoagulated during the simulation. That BC, though, was still internally mixed (with greater than 20% coating) due to S(VI) condensation and subsequent hydration and dissolution. If continuous emissions were treated simultaneously with the processes described here, distribution E1 (BC < 5% shell) would always be present to some degree, as shown by *Jacobson* [2001]. Figure 6d similarly shows that only a small amount of soil remained uncoagulated. Figures 6e–6i show the fate of water, soluble species, and the solid gypsum [$CaSO_4 \cdot 2H_2O$(s)]. Gypsum, which can form when the RH is less than 97%, tied up sulfate in the sea spray, sea spray–sulfate, and mixed distributions, reducing the water contents of those distributions.

6.6. Solid Formation During Diurnal Variation of RH

[51] Figure 7 shows time series concentrations, summed over all sizes, from an additional simulation in which condensation and nucleation of S(VI), dissolution of HCl, HNO_3, and NH_3, equilibrium chemistry of all components, and equilibrium hydration were solved simultaneously over the five initial distributions shown in Figure 1 (except that nucleation was solved for only in the sulfate distribution, D). Coagulation was ignored. The initial gas concentrations of S(VI), HCl, HNO_3, and NH_3 were 1, 0, 0.8, and 0.3 μg m^{-3}, respectively. During the 24 hour simulation, the RH varied sinusoidally from 95 to 5 back to 95%. The temperature was held at 285 K. When the RH was decreasing, a solid was not allowed to form unless it already existed or until the RH decreased below the CRH of the solid. Thus, a metastable state was assumed upon a decrease in RH. When the RH was increasing, a solid was allowed to form (but did not have to form) if the RH was less than the DRH of the solid.

[52] The only solid that could potentially be present at an initial RH of 95% was gypsum [$CaSO_4 \cdot 2H_2O$(s)], which has a DRH of 97%. Figure 7a shows that it formed initially in the sea spray distribution and was present to some degree at all RHs. Figures 7a and 7b show that the water content decreased with decreasing RH and increased with increasing RH, as expected. Water content was higher for a longer period during a decrease in RH than for an increase in RH, particularly in the sea spray distribution, since a metastable state was assumed during a decrease in RH but not an increase. Assuming a metastable reduced solid formation in comparison with not assuming one, increasing liquid water content. The most abundant solids formed in the sea spray distribution were NaCl(s), gypsum, and $NaNO_3$(s). In the sulfate distribution (which did not contain Na^+, Mg^{2+}, Ca^{2+}, or K^+ because coagulation was ignored), the primary solids were NH_4HSO_4(s) and $(NH_4)_2SO_4$(s). Much more NH_4^+ entered the sulfate distribution than the sea spray distribution because the sea spray distribution had more cations there initially. More NO_3^- entered the sea spray distribution than the sulfate distribution for the opposite reason. Although no HCl existed in the gas phase and no Cl^- existed in the sulfate distribution initially, some Cl^- was transferred from the sea spray distribution to the gas phase then to the sulfate distribution, as shown in Figure 7b.

6.7. Refractive Indices and Solution Densities

[53] Figures 8a and 8b show solution and total particle real refractive indices, weight percent solute in solution, solution pH, and solution density for the sea spray distribution (A) after a simulation in which condensation of S(VI), dissolution of HCl, HNO_3, NH_3, internal particle

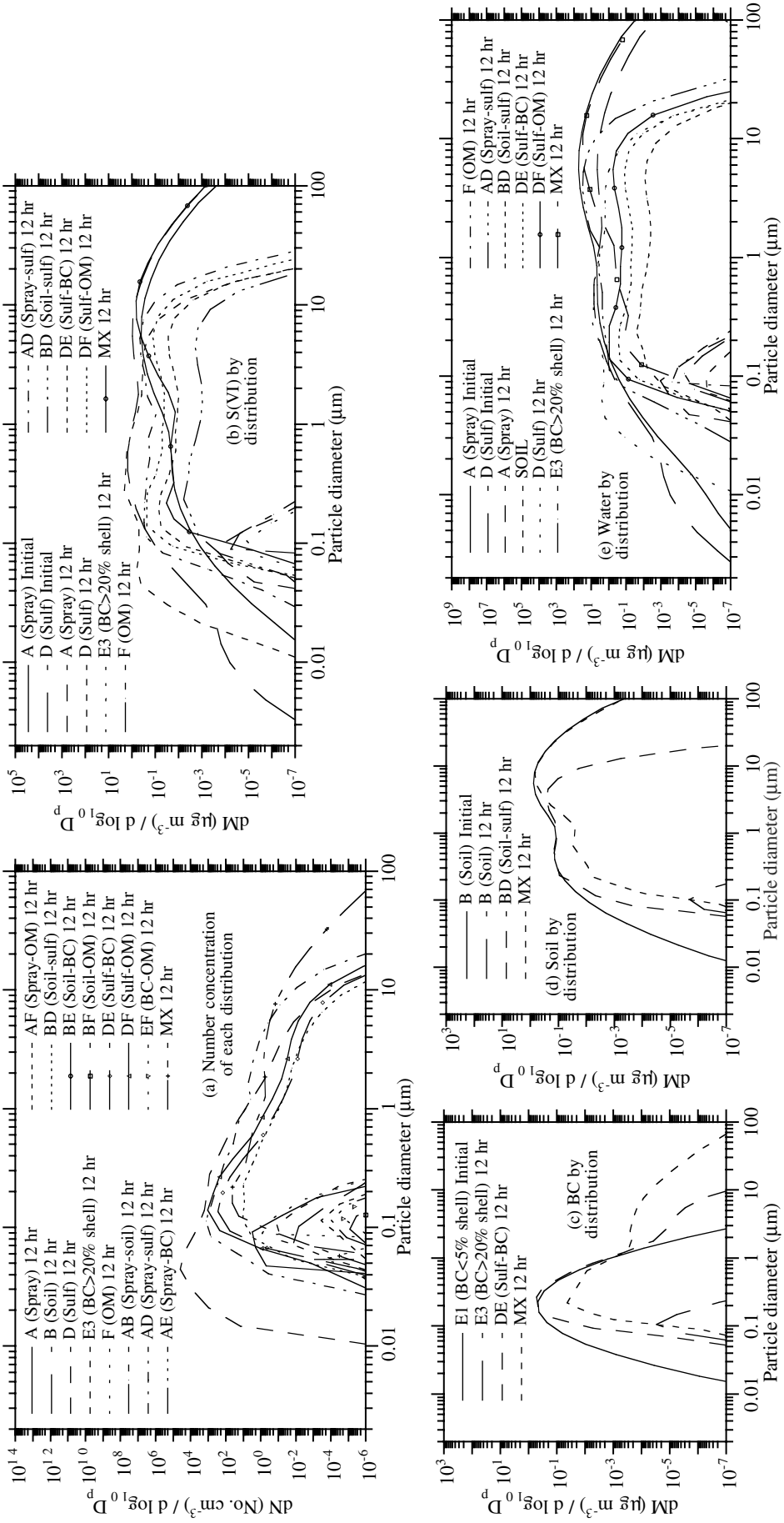

Figure 6. Nucleation, coagulation, condensation, and dissolution/equilibrium. Same as Figure 5, but when coagulation was treated as well. The moving-center structure was used to obtain these results.

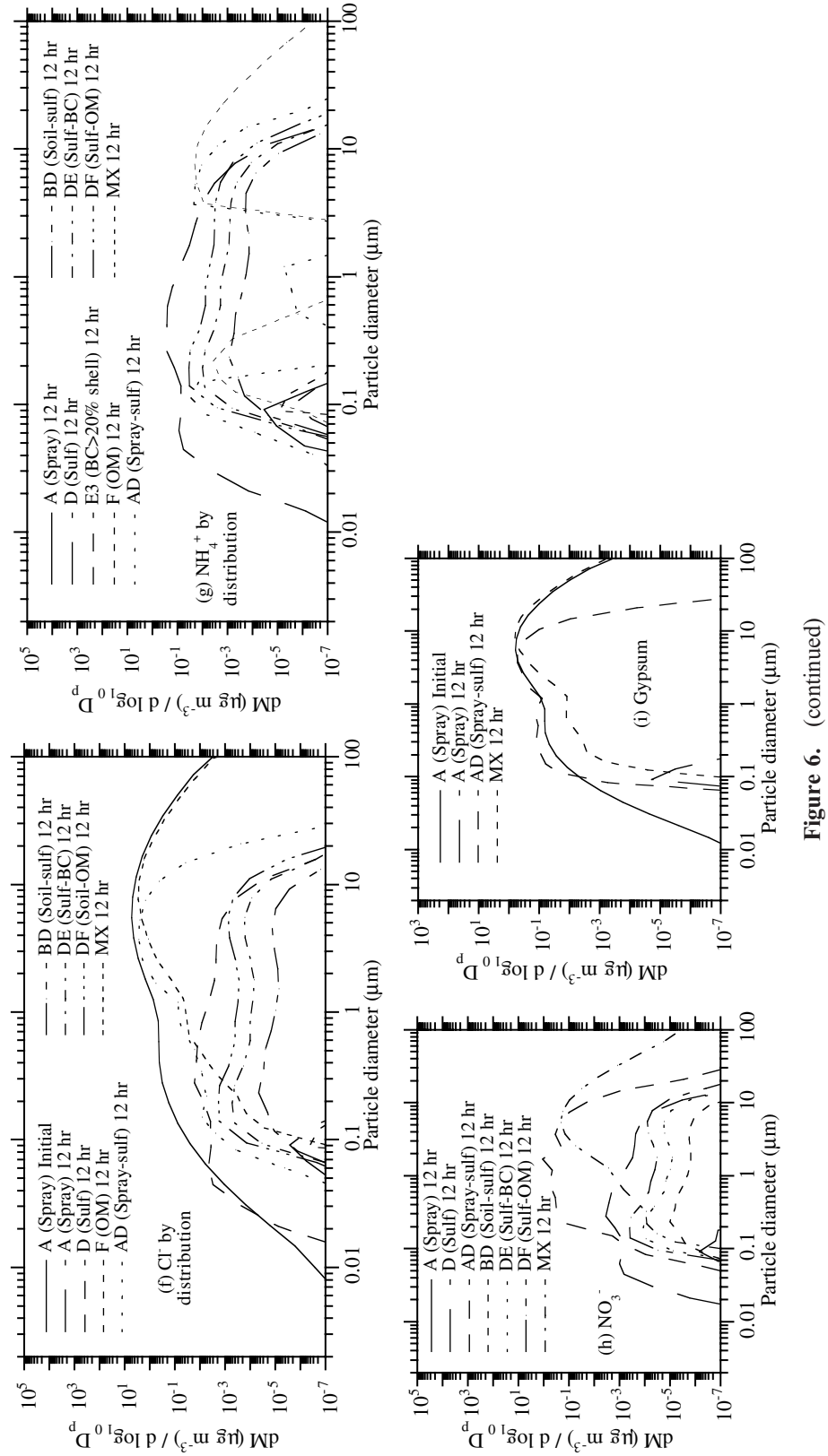

Figure 6. (continued)

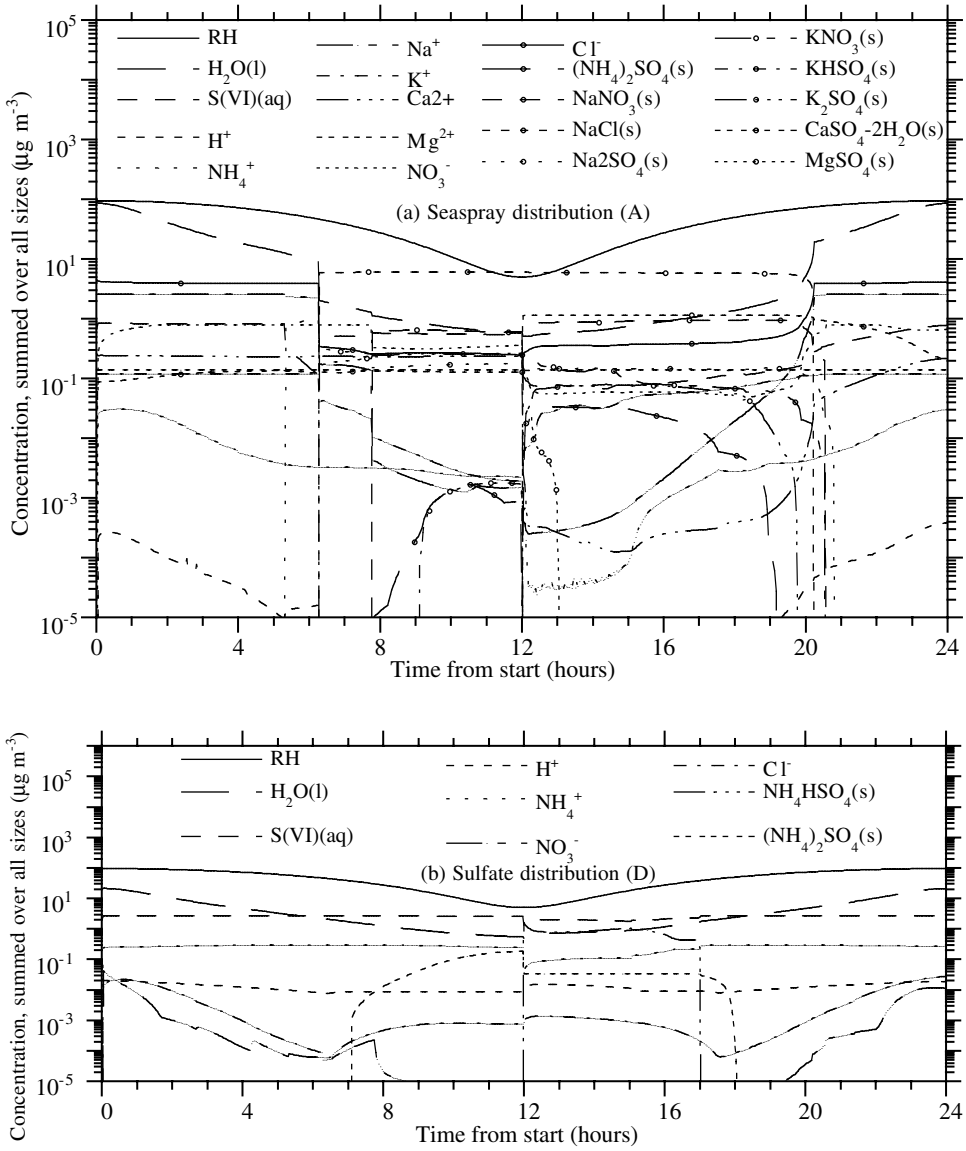

Figure 7. Time variation of concentrations, summed over all size bins, of ions, liquids, and solids in the (a) sea spray distribution and (b) sulfate distribution during a 24 hour simulation in which condensation of S(VI), nucleation of S(VI), dissolution of HCl, HNO_3, and NH_3, equilibrium chemistry of all components, and equilibrium hydration were solved simultaneously over the five initial distributions shown in Figure 1. Coagulation was ignored. The initial gas concentrations of S(VI), HCl, HNO_3, and NH_3 were 1, 0, 0.8, and 0.3 $\mu g\ m^{-3}$, respectively. During the simulation, the RH (also shown) dropped from 95% to 5% then rose again to 95%.

equilibrium, and equilibrium hydration were treated at 90% and 40% RH, respectively. Coagulation was ignored. Figures 8c and 8d show the concentrations of species in the sea spray distribution in the two cases, respectively, at the time of the refractive index calculations. The difference between the solution and total particle refractive indices for the sea spray distribution is the refractive indices due to solids, since they are not in solution.

[54] Figure 8a shows that the difference between solution and total refractive indices at 90% RH was small. This was because the solution volume dominated the total particle volume at 90% RH. The only nonsolution component of the particles in that case was gypsum. The weight percent solute in the distribution peaked at about 0.1 μm diameter. Because water has a lower density and refractive index than do most electrolytes dissolved in solution, solution density and refractive index also peaked at about 0.1 μm.

[55] Figure 8b shows that the increase in weight percent solute with decreasing particle size was greater at 40% RH than at 90% RH, causing the solution density to increase with decreasing particle size more at 40% RH than at 90% RH. At all particle sizes, solids comprised a greater percent of particles at 40% RH than at 90% RH. At 40% RH, the solid fraction increased with decreasing particle size. Due to the high solid fraction at 40% RH, the total particle real refractive index at all particle sizes was about 7% higher than was the solution real refractive index, and both were higher than the total or solution refractive indices at 90%

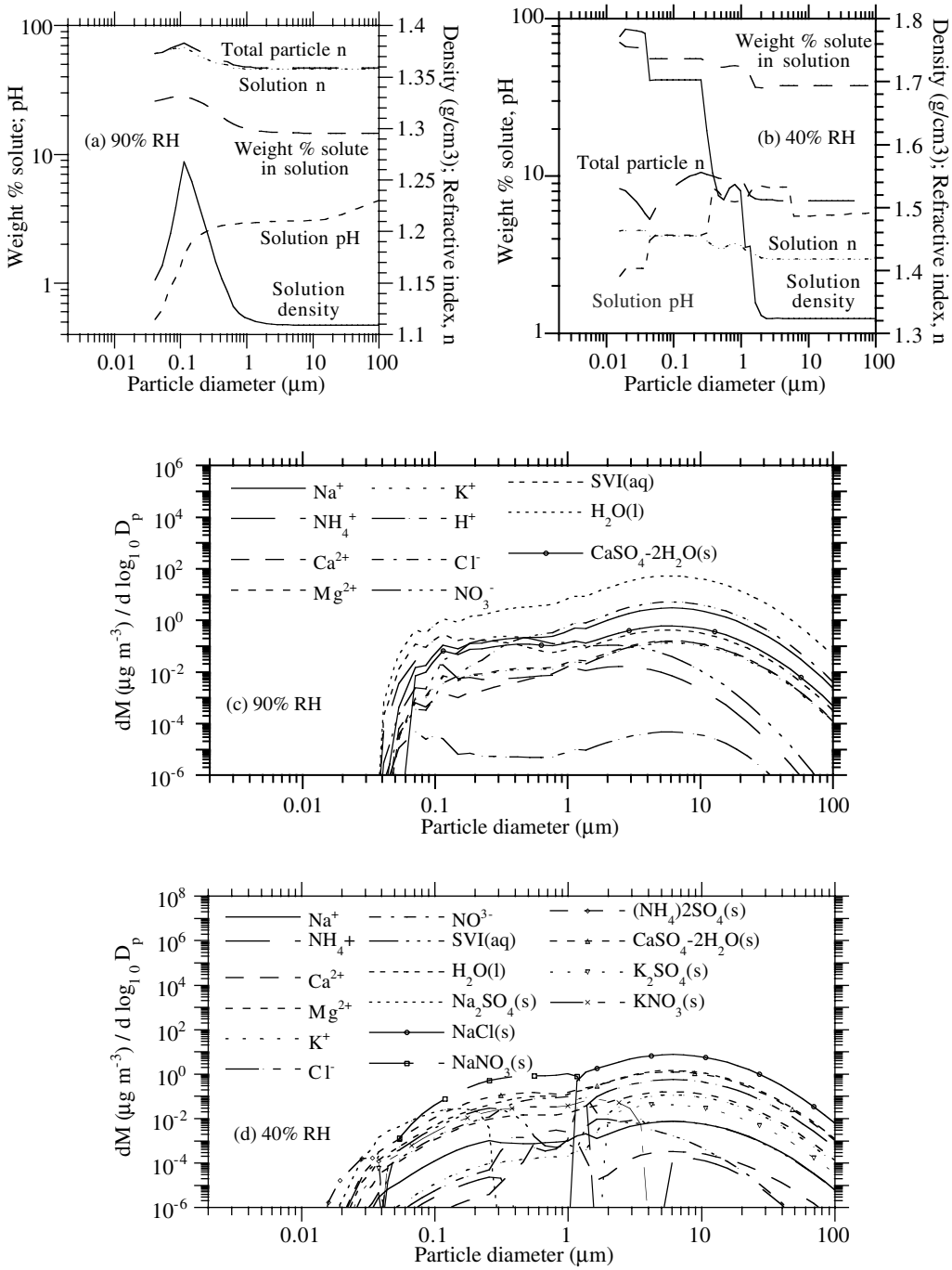

Figure 8. Weight percent solution, pH, solution density, total particle refractive index, and solution refractive index for the sea spray distribution (A) after a simulation in which condensation of S(VI), dissolution of HCl, HNO_3, NH_3, internal particle equilibrium, and equilibrium hydration were treated and when the RH was (a) 90% and (b) 40%. Mass concentrations corresponding to Figures 7a and 7b are given in Figures 7c and 7d, respectively.

RH. Solid electrolytes enhanced the real refractive index compared with when the electrolytes dissolve in solution because when electrolytes dissolved, they hydrated water, and the real refractive index of water is less than that of most solid electrolytes.

[56] Although real refractive indices of particles with solutions decrease with increasing RH, scattering extinction coefficients of such particles increase with increasing RHs [e.g., *Tang et al.*, 1997], because particle cross sections increase with increasing RHs.

7. Conclusions

[57] This paper discussed numerical techniques for solving coagulation, simultaneous nucleation and condensation, and nonequilibrium dissolution/equilibrium reversible chemistry

over multiple size distributions. All schemes conserve moles (including between the gas and aerosol phases) or volume, are unconditionally stable, and except for the reversible chemistry scheme, noniterative. The schemes, previously used in a global 3-D climate study [*Jacobson*, 2001], were applied here in a zero-dimensional box model to analyze the effect of (1) coagulation alone, (2) nucleation plus condensation alone, (3) nucleation, condensation, and coagulation, (4) nucleation, condensation, dissolution/reversible chemistry, and (5) nucleation, condensation, coagulation, dissolution/reversible chemistry, all among multiple aerosol size distributions and the gas phase. Some results of the study were

1. Coagulation internally mixes particles of different original composition over the entire size distribution.
2. Coagulation internally mixes a greater fraction of larger particles than smaller particles.
3. Coagulation internally mixes larger particles with a greater number of other distributions than it does smaller particles.
4. Coagulation among multiple distributions produces the same summed size distribution as coagulation of a single distribution when the sum of the initial distributions are the same in both cases.
5. In a competition for available vapor between homogeneous nucleation and condensation, the relative importance of condensation increases with an increasing number of background particles.
6. In the absence of a continuous source of new particles, coagulation, condensation, dissolution, hydration, and chemical reaction internally mix most particles within half a day under moderately polluted conditions.
7. Condensation increases the fractional coating of small particles more than it does large particles.
8. The real refractive index of a particle containing electrolytes is higher at low RHs than at high RHs.
9. The difference between the real refractive index of a total particle containing electrolytes and its solution component increases with decreasing RH.
10. The real refractive index of a solution generally increases with decreasing particle size.

[58] **Acknowledgments.** This work was supported by the NASA New Investigator Program in Earth Sciences, the Environmental Protection Agency, the National Science Foundation, the David and Lucile Packard Foundation and the Hewlett-Packard Company, and the Stanford University Office of Technology and Licensing.

References

Andreae, M. O., R. J. Charlson, F. Bruynseels, H. Storms, R. V. Grieken, and W. Maenhaut, Internal mixture of sea salt, silicates, and excess sulfate in marine aerosols, *Science*, *232*, 1620–1623, 1986.

Binkowski, F. S., and U. Shankar, The regional particulate matter model, 1, Model description and preliminary results, *J. Geophys. Res.*, *100*, 26,191–26,209, 1995.

Bott, A., A flux method for the numerical solution off the stochastic collection equation: Extension to two-dimensional particle distributions, *J. Atmos. Sci.*, *57*, 284–294, 2000.

Brock, J. R., D. Zehavi, and P. Kuhn, Condensation aerosol formations and growth in a laminar coaxial jet: Experimental, *J. Aerosol Sci.*, *17*, 11–22, 1986.

Capaldo, K. P., C. Pilinis, and S. N. Pandis, A computationally efficient hybrid approach for dynamic gas/aerosol transfer in air quality models, *Atmos. Environ.*, *34*, 3617–3627, 2000.

Celia, M. A., and W. G. Gray, *Numerical Methods for Differential Equations*, Prentice-Hall, Old Tappan, N. J., 1992.

Chock, D. P., and S. L. Winkler, A trajectory-grid approach for solving the condensation and evaporation equations of aerosols, *Atmos. Environ.*, *34*, 2957–2973, 2000.

Fassi-Fihri, A., K. Suhre, and R. Rosset, Internal and external mixing in atmospheric aerosols by coagulation: Impact on the optical and hygroscopic properties of the sulfate-soot system, *Atmos. Environ.*, *31*, 1392–1402, 1997.

Fernandez-Diaz, J. M., M. A. Rodriguez-Brana, C. Gonzalez-Pola, B. Arganza, and P. J. Garcia-Nieto, A modified semi-implicit method to obtain the evolution of an aerosol by coagulation, *Atmos. Environ.*, *34*, 4301–4314, 2000.

Fridlind, A. M., and M. Z. Jacobson, A study of the gas–aerosol equilibrium and aerosol pH in the remote marine boundary layer during the First Aerosol Characterization Experiment (ACE 1), *J. Geophys. Res.*, *105*, 17,325–17,340, 2000.

Friedlander, S. K., Dynamics of aerosol formation by chemical reaction, *Ann. N. Y. Acad. Sci.*, *404*, 354–364, 1983.

Gelbard, F., Modeling multicomponent aerosol particle growth by vapor condensation, *Aerosol Sci. Technol.*, *12*, 399–412, 1990.

Gelbard, F., and J. H. Seinfeld, Simulation of multicomponent aerosol dynamics, *J. Colloid Interface Sci.*, *78*, 485–501, 1980.

Gelbard, F., J. W. Fitzgerald, and W. A. Hoppel, A one-dimensional sectional model to simulate multicomponent aerosol dynamics in the marine boundary layer, 3, Numerical methods and comparisons with exact solutions, *J. Geophys. Res.*, *103*, 16,119–16,132, 1998.

Guazzotti, S. A., J. R. Whiteaker, D. Suess, K. R. Coffee, and K. A. Prather, *Atmos. Environ.*, *35*, 3229–3240, 2001.

Hale, G. M., and M. R. Querry, Optical constants of water in the 200-nm to 200-mm wavelength region, *Appl. Opt.*, *12*, 555–563, 1973.

Jacobson, M. Z., Development and application of a new air pollution modeling system, part II, Aerosol module structure and design, *Atmos. Environ.*, *31*, 131–144, 1997a.

Jacobson, M. Z., Development and application of a new air pollution modeling system, part III, Aerosol-phase simulations, *Atmos. Environ.*, *31*, 587–608, 1997b.

Jacobson, M. Z., Numerical techniques to solve condensational and dissolutional growth equations when growth is coupled to reversible reactions, *Aerosol Sci. Technol.*, *27*, 491–498, 1997c.

Jacobson, M. Z., *Fundamentals of Atmospheric Modeling*, Cambridge Univ. Press, New York, 1999a.

Jacobson, M. Z., Studying the effects of calcium and magnesium on size-distributed nitrate and ammonium with EQUISOLV II, *Atmos. Environ.*, *33*, 3635–3649, 1999b.

Jacobson, M. Z., Isolating nitrated and aromatic aerosols and nitrated aromatic gases as sources of ultraviolet light absorption, *J. Geophys. Res.*, *104*, 3527–3542, 1999c.

Jacobson, M. Z., A physically-based treatment of elemental carbon optics: Implications for global direct forcing of aerosols, *Geophys. Res. Lett.*, *27*, 217–220, 2000.

Jacobson, M. Z., Strong radiative heating due to the mixing state of black carbon in atmospheric aerosols, *Nature*, *409*, 695–697, 2001.

Jacobson, M. Z., and R. P. Turco, Simulating condensational growth, evaporation, and coagulation of aerosols using a combined moving and stationary size grid, *Aerosol Sci. Technol.*, *22*, 73–92, 1995.

Jacobson, M. Z., R. P. Turco, E. J. Jensen, and O. B. Toon, Modeling coagulation among particles of different composition and size, *Atmos. Environ.*, *28A*, 1327–1338, 1994.

Jacobson, M. Z., A. Tabazadeh, and R. P. Turco, Simulating equilibrium within aerosols and nonequilibrium between gases and aerosols, *J. Geophys. Res.*, *101*, 9079–9091, 1996.

Jeong, J. I., and M. Choi, A sectional method for the analysis of growth of polydisperse non-spherical particles undergoing coagulation and coalescence, *J. Aerosol Sci.*, *32*, 565–582, 2001.

Kim, Y. P., and J. H. Seinfeld, Simulation of multicomponent aerosol condensation by the moving sectional method, *J. Colloid Interface Sci.*, *135*, 185–199, 1990.

Kim, Y. P., and J. H. Seinfeld, Simulation of multicomponent aerosol dynamics, *J. Colloid Interface Sci.*, *149*, 425–449, 1992.

Kleeman, M. J., G. R. Cass, and A. Eldering, Modeling the airborne particle complex as a source-oriented external mixture, *J. Geophys. Res.*, *102*, 21,355–21,372, 1997.

Kostoglou, M., and A. J. Karabelas, Evaluation of zero order methods for simulating particle coagulation, *J. Colloid Interface Sci.*, *163*, 420–431, 1994.

Krekov, G. M., Models of atmospheric aerosols, in *Aerosol Effects On Climate*, edited by S. G. Jennings, pp. 9–64, Univ. of Ariz. Press, Tucson, 1993.

Kumar, S., and D. Ramkrishna, On the solution of population balance

equations by discretization, I, A fixed pivot technique, *Chem. Eng. Sci.*, *51*, 1311–1332, 1996.
Levin, Z. L., E. Ganor, and V. Gladstein, The effects of desert particles coated with sulfate on rain formation in the eastern Mediterranean, *J. Appl. Meteorol.*, *35*, 1511–1523, 1996.
Lister, J. D., D. J. Smit, and M. J. Hounslow, Adjustable discretized population balance for growth and aggregation, *AIChE J.*, *41*, 591–603, 1995.
Lushnikov, A. A., Evolution of coagulating systems, *J. Colloid Interface Sci.*, *54*, 94–101, 1975.
Meng, Z., and J. H. Seinfeld, Time scales to achieve atmospheric gas–aerosol equilibrium for volatile species, *Atmos. Environ.*, *30*, 2889–2900, 1996.
Meng, Z., D. Dabdub, and J. H. Seinfeld, Size-resolved and chemically resolved model of atmospheric aerosol dynamics, *J. Geophys. Res.*, *103*, 3419–3435, 1998.
Middleton, P., and J. R. Brock, Simulation of aerosol kinetics, *J. Colloid Interface Sci.*, *54*, 249–264, 1976.
Mordy, W., Computations of the growth by condensation of a population of cloud droplets, *Tellus*, *11*, 16–44, 1959.
Murphy, D. M., J. R. Anderson, P. K. Quinn, L. M. McInnes, F. J. Brechtel, S. M. Kreidenweis, A. M. Middlebrook, M. Pósfai, D. S. Thomson, and P. R. Buseck, Influence of sea-salt on aerosol radiative properties in the Southern Ocean marine boundary layer, *Nature*, *395*, 62–65, 1998.
Naoe, H., and K. Okada, Mixing properties of submicrometer aerosol particles in the urban atmosphere: With regard to soot particles, *Atmos. Environ.*, *35*, 5765–5772, 2001.
Nguyen, K., and D. Dabdub, Two-level time-marching scheme using splines for solving the advection equation, *Atmos. Environ.*, *35*, 1627–1637, 2001.
Okada, K., and R. Hitzenberger, Mixing properties of individual submicrometer particles in Vienna, *Atmos. Environ.*, *35*, 5617–5628, 2001.
Palmer, K. F., and D. Williams, Optical constants of sulfuric acid: Application to the clouds of Venus?, *Appl. Opt.*, *14*, 208–219, 1975.
Pilinis, C., Derivation and numerical solution of the species mass distribution equation for multicomponent particulate systems, *Atmos. Environ.*, *24*, 1923–1928, 1990.
Pilinis, C., K. P. Capaldo, A. Nenes, and S. N. Pandis, MADM: A new multicomponent aerosol dynamics model, *Aerosol Sci. Technol.*, *32*, 482–502, 2000.
Pósfai, M., J. R. Anderson, P. R. Buseck, and H. Sievering, Soot and sulfate aerosol particles in the remote marine troposphere, *J. Geophys. Res.*, *104*, 21,685–21,693, 1999.
Query, M. R., Optical constants of minerals and other materials from the millimeter to the ultraviolet, *CRDEC-CR-88009*, Aberdeen Proving Ground, Maryland, 1987.
Rao, N. P., and P. H. McMurry, Nucleation and growth of aerosol in chemically reacting systems, *Aerosol Sci. Technol.*, *11*, 120–133, 1989.
Russell, L. M., and J. H. Seinfeld, Size- and composition-resolved externally mixed aerosol model, *Aerosol Sci. Technol.*, *28*, 403–416, 1998.
Sandu, A., A Newton–Cotes quadrature approach for solving the aerosol coagulation equation, *Atmos. Environ.*, *36*, 583–589, 2002.
Sandu, A., and C. T. Borden, A framework for the numerical treatment of aerosol dynamics, *Technical Report CSTR-01-03*, Dept. of Comput. Sci., Mich. Tech. Univ., Houghton, Mich., 2001.
Seigneur, C., A model of sulfate aerosol dynamics in atmospheric plumes, *Atmos. Environ.*, *16*, 2207–2228, 1982.
Silva, P. J., R. A. Carlin, and K. A. Prather, Single particle analysis of suspended soil dust from southern California, *Atmos. Environ.*, *34*, 1811–1820, 2000.
Smolarkiewicz, P. K., A simple positive definite advection scheme with small implicit diffusion, *Mon. Weather Rev.*, *111*, 479–486, 1983.
Song, C. H., and G. R. Carmichael, The aging process of naturally emitted aerosol (sea-salt and mineral aerosol) during long range transport, *Atmos. Environ.*, *33*, 2203–2218, 1999.
Stelson, A. W., Urban aerosol refractive index prediction by partial molar refraction approach, *Environ. Sci. Technol.*, *24*, 1676–1679, 1990.
Strom, J., K. Okada, and J. Heintzenberg, On the state of mixing of particles due to Brownian coagulation, *J. Aerosol Sci.*, *23*, 467–480, 1992.
Suck, S. H., and J. R. Brock, Evolution of atmospheric aerosol particle size distributions via Brownian coagulation: Numerical simulation, *J. Aerosol Sci.*, *10*, 581–590, 1979.
Sun, Q., and A. S. Wexler, Modeling urban and regional aerosols: Condensation and evaporation near acid neutrality, *Atmos. Environ.*, *32*, 3527–3531, 1998a.
Sun, O., and A. S. Wexler, Modeling urban and regional aerosols near neutral acidity: Application to the 24–25 June SCAQS episode, *Atmos. Environ.*, *32*, 3533–3545, 1998b.
Toon, O. B., and T. P. Ackerman, Algorithms for the calculation of scattering by stratified spheres, *Appl. Opt.*, *20*, 3657–3660, 1981.
Toon, O. B., J. B. Pollack, and B. N. Khare, The optical constants of several atmospheric aerosol species: Ammonium sulfate, aluminum oxide, and sodium chloride, *J. Geophys. Res.*, *81*, 5733–5748, 1976.
Toon, O. B., R. P. Turco, D. Westphal, R. Malone, and M. S. Liu, A Multidimensional model for aerosols: Description of computational analogs, *J. Atmos. Sci.*, *42*, 2123–2143, 1997.
Tang, I., Thermodynamic and optical properties of mixed-salt aerosols of atmospheric importance, *J. Geophys. Res.*, *102*, 1883–1893, 1997.
Tang, I. N., A. C. Tridico, and K. H. Fung, Thermodynamic and optical properties of sea salt aerosols, *J. Geophys. Res.*, *102*, 23,269–23,275, 1997.
Tsang, T. H., and J. R. Brock, Aerosol coagulation in the plume from a crosswind line source, *Atmos. Environ.*, *16*, 2229–2235, 1982.
Tsang, T. H., and J. R. Brock, Simulation of condensation aerosol growth by condensation and evaporation, *Aerosol Sci. Technol.*, *5*, 385–388, 1986.
Tsang, T. H., and L. K. Huang, On a Petrov–Galerkin finite element method for evaporation of polydisperse aerosols, *Aerosol Sci. Technol.*, *12*, 578–597, 1990.
Tsang, T. H., and N. Korgaonkar, Effect of evaporation on the extinction coefficient of an aerosol cloud, *Aerosol Sci. Technol.*, *7*, 317–328, 1987.
Trautmann, T., and C. Wanner, A fast and efficient modified sectional method for simulating multicomponent collisional kinetics, *Atmos. Environ.*, *33*, 1631–1640, 1999.
Turco, R. P., P. Hamill, O. B. Toon, R. C. Whitten, and C. S. Kiang, The NASA-Ames Research Center stratospheric aerosol model, I, Physical processes and computational analogs, *NASA Tech. Publ. (TP) 1362, iii-94*, 1979.
Tzivion, S., G. Feingold, and Z. Levin, An efficient numerical solution to the stochastic collection equation, *J. Atmos. Sci.*, *44*, 3139–3149, 1987.
Varoglu, E., and W. D. L. Finn, Finite elements incorporating characteristics for one-dimensional diffusion-convection equation, *J. Comput. Phys.*, *34*, 371–389, 1980.
Von Salzen, K., and K. H. Schlünzen, A prognostic physico-chemical model of secondary and marine inorganic multicomponent aerosols, I, Model description, *Atmos. Environ.*, *33*, 567–576, 1999.
Warren, D. R., and J. H. Seinfeld, Simulation of aerosol size distribution evolution in systems with simultaneous nucleation, condensation, and coagulation, *Aerosol Sci. Technol.*, *4*, 31–43, 1985.
Whitby, E. R., The model aerosol dynamics model, part I, *Report to the U.S. Environmental Protection Agency*, Dept. of Mech. Eng., Univ. of Minn., Minneapolis, 1985.
Zhang, Y., C. Seigneur, J. H. Seinfeld, M. Z. Jacobson, and F. Binkowski, Simulation of aerosol dynamics: A comparative review of algorithms used in air quality models, *Aerosol Sci. Technol.*, *31*, 487–514, 1999.

M. Z. Jacobson, Department of Civil and Environmental Engineering, Stanford University, Terman Engineering Center, Room M-31, Stanford, CA 94305-4020, USA. (jacobson@stanford.edu)